



YILDIRIM BEYAZIT UNIVERSITY
GRADUATE SCHOOL OF NATURAL AND APPLIED SCIENCES

**AUTOMATED GRADING AND DIAGNOSIS SYSTEM FOR
EVALUATION OF DRY EYE DISEASE**

**M.Sc. Thesis by
AYŞE ARSLAN**

Department of Computer Engineering

**June, 2015
ANKARA**



Ayşe ARSLAN

Department of Computer Engineering

2016 ANKARA

**AUTOMATED GRADING AND DIAGNOSIS
SYSTEM FOR EVALUATION OF DRY EYE DISEASE**

**A Thesis Submitted to
the Graduate School of Natural and Applied Sciences of Yıldırım Beyazıt
University**

**In Partial Fulfillment of the Requirements for the Degree of Master of Science
in Computer Engineering, Department of Computer Engineering**

by

Ayşe ARSLAN

June, 2016

ANKARA

M.Sc. THESIS EXAMINATION RESULT FORM

We have read the thesis entitled “AUTOMATED GRADING AND DIAGNOSIS SYSTEM FOR EVALUATION OF DRY EYE DISEASE” completed by Ayşe ARSLAN under supervision of Asst. Prof. Dr. Baha ŞEN and we certify that in our opinion it is fully adequate, in scope and in quality, as a thesis for the degree of Master of Science.

.....
Asst. Prof. Dr. Baha ŞEN

(Supervisor)

.....
Prof. Dr. Fatih V. ÇELEBİ

(Jury member)

.....
Asst. Prof. Dr. Mehmet DEMİRER

(Jury Member)

.....
Prof. Dr. Fatih V. ÇELEBİ

(Director)

Graduate School of Natural and Applied Sciences

ETHICAL DECLARATION

I have prepared this dissertation study in accordance with the Rules of Writing Thesis of Yildirim Beyazıt University of Science and Technology Institute;

- Data I have presented in the thesis, information and documents that I obtained in the framework of academic and ethical rules,
- All information, documentation, assessment and results that I presented in accordance with scientific ethics and morals,
- I have gave references all the works that I were benefited in this dissertation by appropriate reference,
- I would not make any changes in the data that I were used,
- The work presented in this dissertation I would agree that the original,

I state, in the contrary case I declare that I accept the all rights losses that may arise against me.

ACKNOWLEDGEMENTS

Firstly, I would like to express my sincere gratitude to my advisor Asst. Prof. Dr. Baha Şen for the support of my thesis study and related research, for his highly motivation, immense knowledge and constructive recommendations. His guidance helped me in all the time of research and writing of this thesis.

I would like to thank: Prof. Dr. Fatih Çelebi, Asst. Prof. Dr. Mehmet Demirer and Asst. Prof. Dr. Hilal Kaya for their valuable contribution.

I would like to thank to Yıldırım Beyazıt University Ataturk Education and Research Hospital board to collect the digital DES image dataset. My sincere thanks also goes to Dr. Hasan Basri Çakmak and Dr. Betül Seher Uysal who provided me an opportunity to choose this topic, and for their help in conducting the clinical processes.

Finally, I must express my very profound gratitude to my parents for providing me with unfailing support and continuous encouragement throughout my years of study and through the process of researching and writing this thesis. This accomplishment would not have been possible without them. Thank you.

2016, 2 June

Ayşe ARSLAN

AUTOMATED GRADING AND DIAGNOSIS SYSTEM FOR EVALUATION OF DRY EYE DISEASE

ABSTRACT

Today, Dry Eye Syndrome (DES) is a widely seen health problem that is a disorder of the tear film due to tear deficiency. The number of dry punctate dots occurred on corneal surface can be used as a diagnostic indicator of DES severity. Grading of DES severity exactly by counting these dots is a really difficult task for human eye. Taking into account that current methods are also subjectively dependent on the perception of the ophthalmologists in addition to spending time and resource intensively, the enhancement of diagnosis techniques would significantly contribute to clinical DES analysis.

Computer-aided diagnosis systems can potentially provide more objective and reliable diagnostic results for health care systems. Moreover, they would also benefit as remote diagnosis systems in places where there may not be well-trained ophthalmologists and modern testing techniques. A computerized diagnosis system by utilizing image processing techniques can be developed and used as an automated grading system in clinical decision making, also speed up evaluation, diagnosis and treatment processes.

The work presented in this thesis consists of developing an automated grading system in order to provide more reliable and accurate diagnosis for DES. For determining the recognition performance of the system, an original clinical database has been formed during a year in eye clinic. A computerized diagnosis system is performed at the region of interest (ROI) level by applying computational methods on the fluorescein-stained corneal images. These images were gathered via slit lamp photography after sodium fluorescein staining and labeled based on the clinical Oxford Grading Schema (OGS) traditionally implemented by ophthalmologists that uses a 0-none to 5-severe grading scale.

This study shows that automatic DES diagnostic kits can be developed by implementing computational methods on the fluorescein-stained cornea images to assist investigators for a more objective and faster DES diagnosis in real life.

Keywords

Dry eye syndrome, computer-aided diagnostic system, image processing, clinical grading, classification



KURU GÖZ HASTALIĞININ DEĞERLENDİRİLMESİ İÇİN OTOMATİK SINIFLANDIRMA VE TANI SİSTEMİ

ÖZET

Bugün, gözyaşı eksikliğinden kaynaklanan bir gözyaşı filmi bozukluğu olan Kuru Göz Sendromu (KGS) yaygın olarak görülen bir sağlık sorunudur. Kornea yüzeyi üzerinde oluşan kuru noktaların sayısı KGS şiddetinin bir tanı göstergesi olarak kullanılabilir. KGS şiddetinin bu noktaların tam bir şekilde sayılmasıyla derecelendirilmesi insan gözü için fiilen zor bir işlemdir. Mevcut yöntemlerin yoğun bir şekilde zaman ve kaynak tüketmesinin yanı sıra aynı zamanda oldukça subjektif bir şekilde hekimin algısına bağımlı olduğu düşünülerek, tanı tekniklerinin iyileştirilmesi klinik KGS analizine önemli ölçüde katkı sağlayacaktır.

Bilgisayar destekli sistemler sağlık sistemleri için potansiyel olarak daha objektif ve güvenilir tanı sonuçları sağlayabilir. Dahası, bu sistemler iyi eğitilmiş göz hekimleri ve modern test teknikleri bulunmayan yerlerde uzaktan tanı sistemi olarak faydalı olacaktır. Bilgisayarlı bir teşhis sistemi görüntü işleme teknikleri kullanılarak geliştirilebilir ve klinik karar verme sürecinde otomatik bir derecelendirme şeması olarak kullanılabilir, ayrıca değerlendirme, tanı ve tedavi süreçlerini hızlandırabilir.

Bu tezde sunulan çalışma KGS için daha güvenilir ve kesin tanısını sağlamak için otomatik bir derecelendirme sisteminin geliştirilmesini kapsar. Sistemin tanıma performansının belirlenmesi için orjinal bir klinik veri tabanı göz kliniğinde bir yıl boyunca oluşturulmuştur. Floresein-boyanmış kornea resimleri üzerinde bilgisayarlı methodlar uygulayarak ilgi bölgesi düzeyinde bilgisayarlı bir tanı sistemi gerçekleştirilmiştir. Bu görüntüler, sodyum floresein boyama yapıldıktan sonra biyomikroskop fotoğraflama aracılığıyla toplanmış ve göz hekimleri tarafından geleneksel uygulanan; 0-hiçbiri - 5-şiddetli derecelendirme skalası kullanan klinik Oxford derecelendirme şemasına dayalı olarak etiketlenmiştir.

Açıkça görülebilir ki; ideal floresein boyanmış kornea görüntüleri üzerinde çalışarak ve bilgisayarlı yöntemleri uygulayarak gerçek hayatta araştırmacılara daha objektif

ve daha hızlı KGS tanısında yardımcı olmak için otomatik KGS tanı kitleri geliştirilebilir.

Anahtar Kelimeler

Kuru göz sendromu, bilgisayar destekli tanı sistemi, görüntü işleme, klinik derecelendirme, sınıflandırma.



CONTENTS

M.Sc. THESIS EXAMINATION RESULT FORM	ii
ETHICAL DECLARATION	iii
ACKNOWLEDGEMENTS.....	vii
ABSTRACT.....	v
ÖZET.....	vii
CONTENTS.....	ix
ABBREVIATION	xi
LIST OF TABLES	xii
LIST OF FIGURES	xiii
CHAPTER 1 - INTRODUCTION.....	1
1.1. The Tear Film	2
1.2. The Dry Eye Syndrome	3
1.3. Clinical Evaluation.....	5
1.3.1. The Schirmer Test	5
1.3.2. Ocular Surface Disease Index	6
1.3.3. The Tear Break Up Test	8
1.3.4. Ocular Surface Staining.....	9
1.3.4.1. The Sodium Fluorescein Staining	10
1.3.4.2. The Rose Bengal Staining	11
1.3.4.3. The Lissamine Green Staining	12
1.4. Oxford Grading Schema	12
1.5. Related Works.....	14
1.6. Aim of the Work.....	16
1.7. Motivation.....	17
1.7. Outline.....	17
CHAPTER 2 - MATERIAL AND METHODS.....	18
2.1. Data Acquisition	19
2.2. Extraction of Region of Interest.....	21

2.2.1. Semi-automatic Detection of Region of Interest	22
2.2.2. Full-automatic Detection of Region of Interest.....	22
2.2.2.1. Hough Transform	23
2.3. Processing of ROI.....	26
2.4. Connected Component Labeling.....	27
2.5. Statistical Methods.....	31
CHAPTER 3 - IMPLEMENTATION.....	32
3.1. Conduct of Staining	34
3.2. Image Capture Technique	34
3.3. Clinical Grading.....	35
3.4. Selection of Region of Interest	35
3.4.1. Semi-automatic Detection of Region of Interest.....	37
3.4.2. Full-automatic Detection of Region of Interest.....	37
3.5. Automated Oxford Grading Schema	44
CHAPTER 4 - RESULTS.....	49
CHAPTER 5 - FUTURE WORK AND CONCLUSION	52
CHAPTER 6 - DISCUSSION	53
REFERENCES.....	55
APPENDICES	63
RESUME.....	69

ABBREVIATION

ADDE	Aqueous Tear-Deficient Dry Eye
BUT	Break-up Time
CCC	Concordance Correlation Coefficient
CHT	Circular Hough Transform
DES	Dry Eye Syndrome
DoG	Difference of Gaussians
DT	Decision Tree
EDE	Evaporative Dry Eye
HOS	Higher Order Spectra
HSV	Hue-saturation-value
KNN	K-Nearest Neighbor
NBC	Naïve Bayesian Classifier
NEI	National Eye Institute/Industry
NIBUT	Non-Invasive Break-up Time
OGS	Oxford Grading Schema
OSDI	Ocular Surface Disease Index
RGB	Red-green-blue
ROI	Region of Interest
SVM	Support Vector Machine

LIST OF TABLES

Table 3.1 Arguments of iris detector module and their values.....	39
Table 3.2 Quantative analysis results of each dry blob reported at the end of computational methods in Figure 3.13 and grading as grade 1.....	48
Table 3.3 Quantative analysis results of each dry blob reported at the end of computational methods in Figure 3.14 and grading as grade 2.....	48
Table 4.1 Lin’s Concordance Results	51
Table A.1 Quantative analysis results of each dry blob reported at the end of computational methods in Figure A.1 and grading as grade 3.....	65
Table B.1 Quantative analysis results of each dry blob reported at the end of computational methods in Figure A.2 and grading as grade 1.....	68



LIST OF FIGURES

Figure 1.1 Schematic demonstration of the human eye [1].....	1
Figure 1.2 Trilaminar structure of the tear film [1].....	2
Figure 1.3 Major etiological causes of dry eye [27]	4
Figure 1.4 The Schirmer test in use [1].....	6
Figure 1.5 Ocular surface disease index (OSDI) questionnaire	7
Figure 1.6 Assessment of OSDI questionnaire on a scale of 0 to 100	8
Figure 1.7 Formation of dark areas related to BUT [1]	9
Figure 1.8 (A) Biomicroscopic examination with a slit lamp [5], (B) dryness appearance of fluorescein-stained cornea under cobalt blue filter	10
Figure 1.9 (A) Punctate fluorescein staining, (B) assessment of rose bengal staining [29]	11
Figure 1.10 Staining of the same eye with (A) fluorescein and (B) lissamine green [29].....	12
Figure 1.11 Oxford grading schema [29].....	13
Figure 2.1 Decision making process of fluorescein stained corneal images.....	19
Figure 2.2 Topcon DC-3 digital camera used in data collection process.....	20
Figure 2.3 Iris samples of (A) - (B) clinical dataset; (C) UBIRIS; (D) CASIA.....	21
Figure 2.4 Flowchart of CHT.....	24
Figure 2.5 a) An eye image of the CASIA database b) corresponding edge map c) edge map with only horizontal gradients d) edge map with only vertical gradients [50].....	25
Figure 2.6 a) Pixel p and its 4-neighbors, b) the union of 4-neighbors and diagonal neighbors of pixel p.....	29
Figure 2.7 Connected components a) four 4-connected components b) two 8-connected components c) label matrix obtained using 4-connectivity d) label matrix obtained using 8-connectivity.	30
Figure 3.1 Flowchart of the implemented study	33
Figure 3.2 Eliminated samples from dataset because of having an another epithelium defect	34
Figure 3.3 Grading of staining patterns, (A) grade 1, (B) grade 2, (C) grade 3, (D) grade 3	36
Figure 3.4 (A) Digital image of the fluorescein-stained cornea under cobalt blue filter, user selects a region as ROI by clicking four points, (B) cropping of the selected ROI	38
Figure 3.5 (A) An image of CASIA dataset (B) An image of clinical dataset	39

Figure 3.6 (A) An eye image from the clinical dataset, (B) corresponding edge map	40
Figure 3.7 (A) An eye image from the CASIA database, (B) corresponding edge map	40
Figure 3.8 Automatic detecting iris and pupil boundaries (white circles) on an image of CASIA	41
Figure 3.9 Automatic detection of iris boundaries (red circle) on clinical dataset, A, B, C, D, E, F are successful segmentation; G, H are unsuccessful segmentation.....	42
Figure 3.10 Automatic cropping ROI on an image of clinical dataset.....	44
Figure 3.11 Removing specular flash artifacts occurred within the iris region.....	44
Figure 3.12 Extracting green channel, and transforming rgb to gray, background normalization.....	45
Figure 3.13 (a) Detection of iris boundaries as ROI full-automatically (red circle). (b) extraction of ROI (c) reflection removal (d) binary image after pre-processing the image (extraction of the green channel, image normalization with background smoothing, thresholding) (e) identifying individual dry areas by seeing which pixels are connected to each other and assigning each distinct dry area a different color (d) determining the borders of all the dry areas (f) counting of punctate dot number.....	46
Figure 3.14 (a) Cropping of the digital image of the inferior cornea based on the ROI defined semi-automatically (red circle). (b) binary image after pre-processing the image (extraction of the green channel, image normalization with background smoothing, thresholding) (c) identifying individual dry areas by seeing which pixels are connected to each other and assigning each distinct dry area a different color (d) determining the borders of all the dry areas (e) counting of punctate dot number. ...	47
Figure 4.1 Individual clinical staining scores for all 70 images versus automatically detected punctate dot number (N_{dots}); per linear regression $G_{pred} = 1.3244 \log(N_{dots}) - 0.0612$	50
Figure 4.2 Bland-Altman analysis of clinical grading (C) and automated grading (G_{pred}), average grading against grading difference for all images (n = 1–70).....	50
Figure A.1 Grading a sample in grade 3 based on counted dot number and area.....	64
Figure B.1 Grading a sample in grade 1 based on counted dot number and area.....	67

CHAPTER 1

INTRODUCTION

The eye is the crucial and sensitive sense organ due to being the basis of the sight by transforming the light energy into electrical signals that are sent to the brain via the optic nerve. The eyeball is a slightly asymmetrical globe composed of three tunics; the first and most inner tunic is the retina; the second one is composed of the choroid, the ciliary body and the iris; and, finally, the third and external tunic is formed by the sclera and the cornea (Figure 1.1) [1].

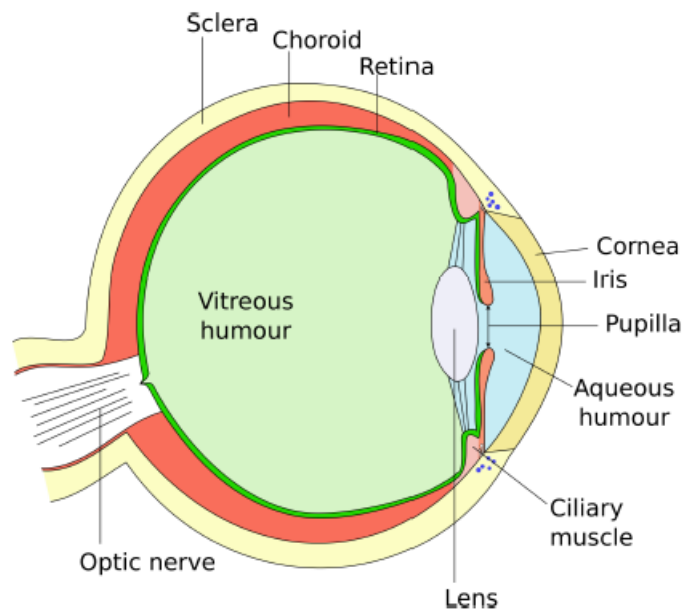


Figure 1.1 Schematic demonstration of the human eye [1]

The cornea is a transparent structure found in the very front of the eye that helps to focus incoming light. There are more nerve endings in the cornea than anywhere else in the body, so it is extremely sensitive. To remain healthy, the cells of the corneal epithelium must be kept moist. This need is met by the elaboration of a thin layer of lubricating substances known as the precorneal tear film. The lacrimal glands,

located in the upper, outer portion of each orbit, secrete the tears, which flow through the main excretory ducts into the space between the eyeball and lids. When a blink occurs, the lacrimal fluid is spread, cleaning and lubricating the surface of the eyes [2].

1.1. The Tear Film

The tear film, which is the interface between the external environment and the ocular surface, has several differing functions [3]. It forms a smooth refracting surface over corneal surface and lubricates the eyelids. Moreover, it maintains an optimal extracellular composition, osmolarity, pH, O₂ and CO₂ levels, nutrient levels, and concentration of growth factors in the tears is regulated within narrow limits [3]. Tears dilute and wash away noxious stimuli, also provide an antibacterial system for the ocular surface [3, 4]. The tear film is an essential component of the eye that plays important functions to guarantee a high optical quality vision [5].

As the tear film has many and varied functions such as lubrication, visual, cleaning, nutritive and antimicrobial functions, it has a complex and dynamic structure of lipids, proteins and mucins covering the anterior surface of the cornea [1]. As shown in Figure 1.2, the tear film has three main components: lipid layer, aqueous layer, mucin layer that provide tear film stabilization, protection from evaporation, electrostatic attraction, optimal spreading and improved ocular absorption [6].

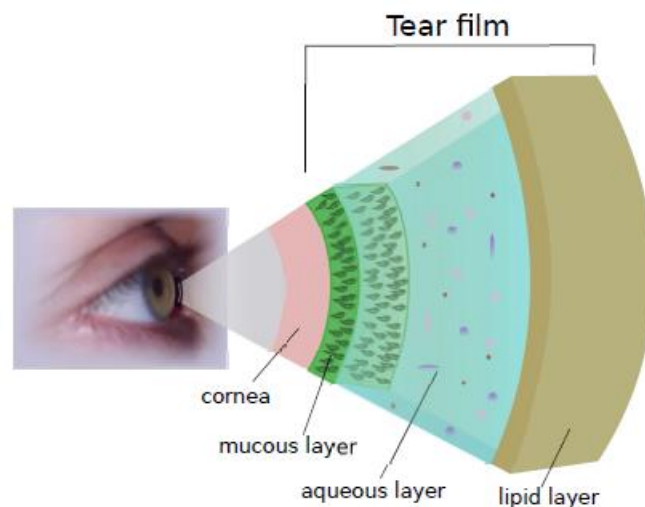


Figure 1.2 Trilaminar structure of the tear film [1]

1.2. The Dry Eye Syndrome

In [7], DES defined as: DES is a disease of the ocular surface which associated with signs of visual discomfort [8-12], lack of tear production [13, 14] and damage risk to the corneal surface. It causes increase in tear film osmolarity [15-17] and ocular surface inflammation [18].

Today, DES is one of the widely seen eye health problems. Epidemiological studies indicate that DES affecting millions of people around the world is a growing public health problem and the prevalence of this syndrome in Turkey is ranged from 10% to 25% according to 45% of ophthalmologists and 25% to 50% according to 25% of ophthalmologists who joined to the study. Several factors, such as age, adverse environmental conditions, use of certain medications, or visual tasks that reduce blink rate, have contributed to that increment [19,20].

DES that is a disorder of the tear film due to tear deficiency or excessive tear evaporation can be classified in two major categories depending on the given causes of the disease (Figure 1.3); Aqueous Tear-Deficient Dry Eye (ADDE) and Evaporative Dry Eye (EDE) [7]. ADDE is due to a failure of lacrimal tear secretion while EDE is caused by excessive water loss from the exposed ocular surface in the presence of normal lacrimal secretory function [1]. If blink rate, an significant factor in tear film stability, is reduced the ocular surface is exposed to water loss and the tear film evaporation is increased. Use of contact lenses may also cause dry eye because it disrupts the tear film [21].

The left yellow box in Figure 1.3 shows the effect of environment on the risk of individuals to be exposed DES. The term “environment” means that external conditions which may cause beginning of DES. Aqueous-deficient dry eye has two primary subsets, these are Sjogren and non-Sjogren DES. Evaporative dry eye has also two subsets, these are intrinsic and extrinsic. Intrinsic evaporative dry eye is occurred where the regulation of evaporative loss from the tear film is directly affected by low blink rate, meibomian lipid deficiency, poor lid dynamics, and the effects of drug action. Extrinsic evaporative dry eye where the regulation of evaporative loss from the tear film is directly affected by increasing evaporation due

to pathological effects on the ocular surface such as vitamin A deficiency, the action of toxic topical agents, contact lens wear and a range of allergic eye diseases. Further details are given in the [27].

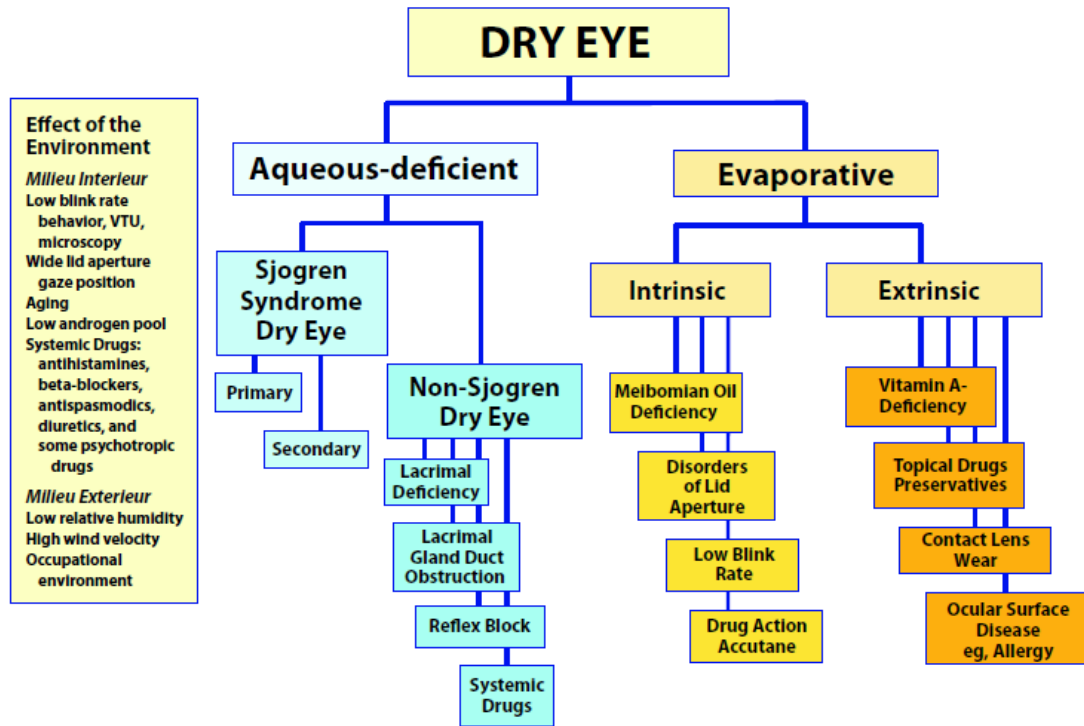


Figure 1.3 Major etiological causes of dry eye [27]

Dry eye is broken down into different diagnostic categories. Regardless of these categories, the symptoms of DES and clinical indications are similar. A reasonable visualization of the familiar processes serves a cycle of decreased tear production or increased evaporation, ocular surface damage, development of signs&symptoms, inflammation, continuation of these process, and complaints of irritation of eye.

DES has a negatively effect on the quality of life with its irritative symptoms on the cornea such as pain, blurry vision, redness, lost of contrast sensitivity, ocular discomforts [22]. DES degrades visual performance in daily common activities such as reading, use of computer, watching and driving significantly, since it can cause deterioration on the corneal surface [23]. It may be seen with increase in concentration of the solution of the tear film and risk of corneal surface inflammation as ocular surgery outcomes [6].

1.3. Clinical Evaluation

In clinical evaluation, ophthalmologists need many tough and time-consuming clinical tests applied to patient to assess the tear film and to diagnose DES clearly, and most of these tests have high variability and low repeatability [7]. Evaluation of cornea structure and dysfunctions subjectively depends on ability and experience of the ophthalmologists.

There are different types of DES diagnosis tests based on assessed parameter type of the tear film. In preliminary evaluation, techniques of DES questionnaires are used in different ways. Quantitative tests of clinical assessment are to evaluate the tear secretion while qualitative tests are to evaluate the tear film stability. Laboratory tests are regarded with the tear film composition; osmolarity analysis and biomicroscopic examination can be also utilized as an important indicator of dryness.

DES severity can be measured based on subjective or objective evaluation. Subjective evaluation depending on visual symptoms cannot ensure consistency because the symptoms and histories of dry eye patients vary widely [24]. Objective evaluation consists of some traditional tests such as Schirmer test, lacrimal river width, tear fern test. There are less invasive evaluations based on tear hyperosmolarity, tear film instability and inflammation. Ocular surface and inflammation can be evaluated conjunctival staining, corneal staining, Meibomian gland evaluation or other tests [6]. The widely used clinical methods for grading DES can be listed as follows:

- Schirmer test,
- Eye questionnaires, such as ocular surface disease index (OSDI),
- The tear break-up time (BUT) test,
- The fluorescein green staining of the corneal surface.

1.3.1. The Schirmer Test

The Schirmer test is a simple way to measure ocular tear generation and DES severity. Standardized strip of filter paper is placed inside the conjunctival sac and the patient closes the eyes (Figure 1.4). Normal tear formation wets this strip

spontaneously by extending downward (at least 15 mm from the eyelid) over a 5 minute period [25]. After that time the length of wet strip is measured. Less than 15 mm of wetting shows tear formation deficiency. Although schirmer test is widely used, some patients may find it very uncomfortable since the patient has to be exposed a strip in eye during several minutes.



Figure 1.4 The Schirmer test in use [1]

1.3.2. Ocular Surface Disease Index (OSDI)

OSDI is a widely used preliminary evaluation questionnaire of DES. Ocular discomfort symptoms such as pain, blurred vision, itching, tearing, and photophobia are analyzed in different conditions of daily life under different humidity and lighting circumstances [1]. Frequency of each symptom are asked patients by offering four options to answer, i.e. never, rarely, sometimes, often/all the times. As a result, reports are obtained about patient complaints. If a patient shows one/more symptoms in often/all the times option, they are thought as symptomatic patients [26]. The questions of OSDI are shown in Figure 1.5 while how the doctors assess the OSDI score for DES severity is shown in Figure 1.6. Though OSDI questionnaire is not a reliable measurement of DES severity when used alone, it is an helpful indicator.

Ocular Surface Disease Index[®] (OSDI[®])²

Ask your patient the following 12 questions, and circle the number in the box that best represents each answer. Then, fill in boxes A, B, C, D, and E according to the instructions beside each.

HAVE YOU EXPERIENCED ANY OF THE FOLLOWING DURING THE LAST WEEK:

	All of the time	Most of the time	Half of the time	Some of the time	None of the time
1. Eyes that are sensitive to light?	4	3	2	1	0
2. Eyes that feel gritty?	4	3	2	1	0
3. Painful or sore eyes?	4	3	2	1	0
4. Blurred vision?	4	3	2	1	0
5. Poor vision?	4	3	2	1	0

Subtotal score for answers 1 to 5

HAVE PROBLEMS WITH YOUR EYES LIMITED YOU IN PERFORMING ANY OF THE FOLLOWING DURING THE LAST WEEK:

	All of the time	Most of the time	Half of the time	Some of the time	None of the time	
6. Reading?	4	3	2	1	0	N/A
7. Driving at night?	4	3	2	1	0	N/A
8. Working with a computer or bank machine (ATM)?	4	3	2	1	0	N/A
9. Watching TV?	4	3	2	1	0	N/A

Subtotal score for answers 6 to 9

HAVE YOUR EYES FELT UNCOMFORTABLE IN ANY OF THE FOLLOWING SITUATIONS DURING THE LAST WEEK:

	All of the time	Most of the time	Half of the time	Some of the time	None of the time	
10. Windy conditions?	4	3	2	1	0	N/A
11. Places or areas with low humidity (very dry)?	4	3	2	1	0	N/A
12. Areas that are air conditioned?	4	3	2	1	0	N/A

Subtotal score for answers 10 to 12

ADD SUBTOTALS A, B, AND C TO OBTAIN D
(D = SUM OF SCORES FOR ALL QUESTIONS ANSWERED)

TOTAL NUMBER OF QUESTIONS ANSWERED
(DO NOT INCLUDE QUESTIONS ANSWERED N/A)

Please turn over the questionnaire to calculate the patient's final OSDI[®] score.

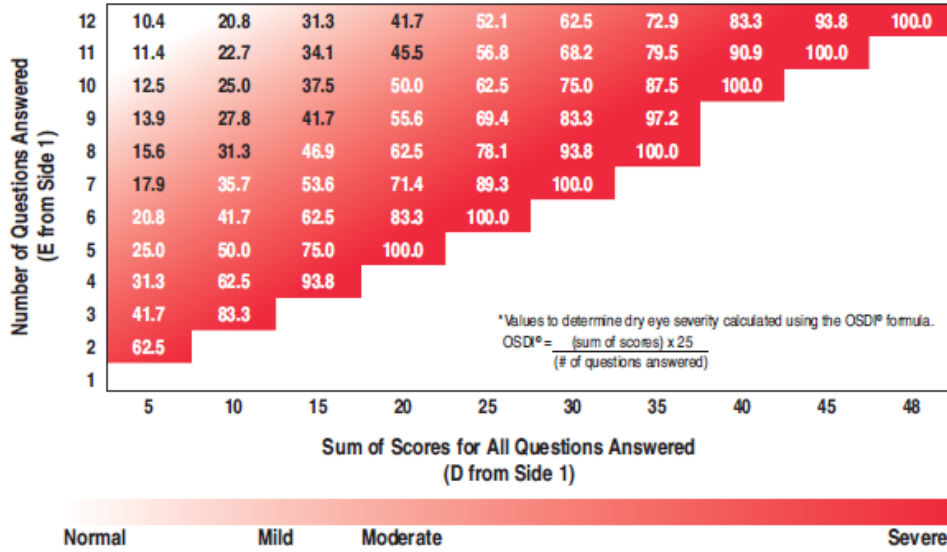
Figure 1.5 Ocular surface disease index (OSDI) questionnaire

Evaluating the OSDI® Score¹

The OSDI® is assessed on a scale of 0 to 100, with higher scores representing greater disability. The index demonstrates sensitivity and specificity in distinguishing between normal subjects and patients with dry eye disease. The OSDI® is a valid and reliable instrument for measuring dry eye disease (normal, mild to moderate, and severe) and effect on vision-related function.

Assessing Your Patient's Dry Eye Disease^{1,2}

Use your answers D and E from side 1 to compare the sum of scores for all questions answered (D) and the number of questions answered (E) with the chart below.* Find where your patient's score would fall. Match the corresponding shade of red to the key below to determine whether your patient's score indicates normal, mild, moderate, or severe dry eye disease.



.....

Patient's Name: _____ Date: _____

How long has the patient experienced dry eye disease? _____

Eye Care Professional's Comments: _____

1. Data on file, Allergan, Inc.
 2. Schiffman RM, Christianson MD, Jacobsen G, Hirsch JD, Reis BL. Reliability and validity of the Ocular Surface Disease Index. *Arch Ophthalmol.* 2000;118:615-621

Copyright © 1995, Allergan

Figure 1.6 Assessment of OSDI questionnaire on a scale of 0 to 100

1.3.3. The Tear Break-Up Test

Tear film stability can be evaluated with tear Break-Up Test (BUT). Moistened fluorescein strips are applied to the lower fornix with minimal stimuli. Patients are asked to blink several times for a few seconds. After making sure that the dye is

homogenously distributed, the time interval between the latest blink and the occurrence of the first corneal black spot is measured three times using slit lamp microscopy with a cobalt blue filter (Figure 1.7). An average reading of three measurements less than 10 seconds is considered to be an indicator of DES [27].

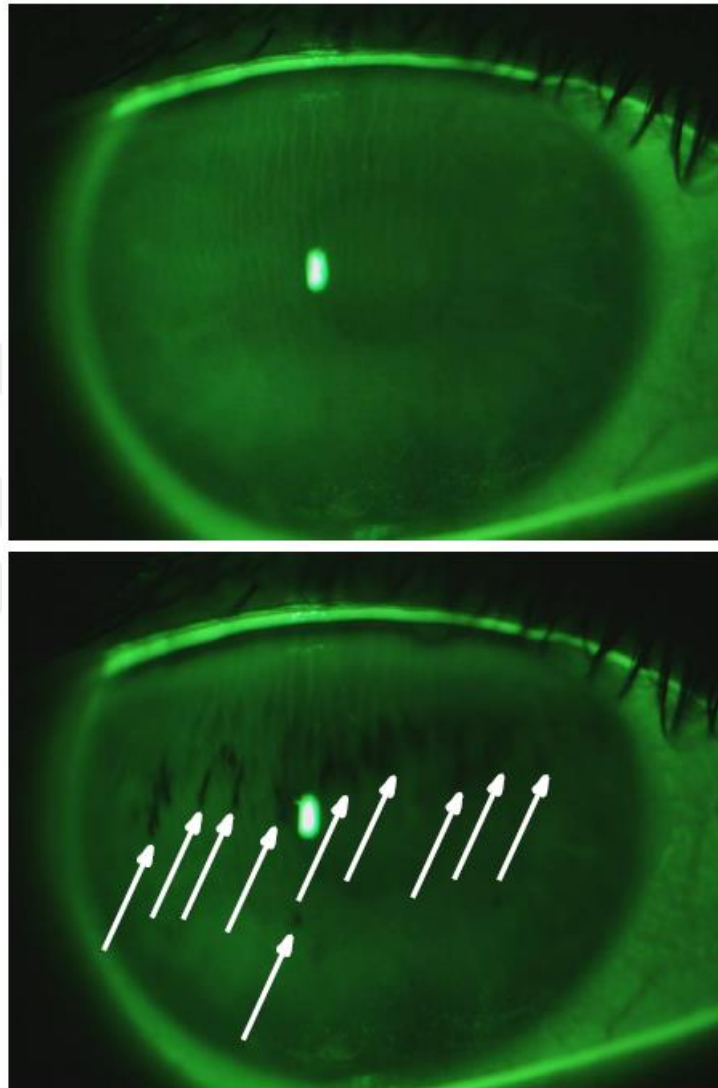


Figure 1.7 Formation of dark areas related to BUT [1]

1.3.4. Ocular Surface Staining

Corneal surface staining is an indicative sign of epithelial damage. The clinical DES assessment widely utilizes usefulness of biomicroscopic examination for grading of corneal surface staining with a biomicroscope system based on a clinical grading scale. Anterior eye can be observed by this system with high magnification under slit

lamp illumination technique after implementation of a staining method, as shown in Figure 1.8.A. The biomicroscope observation has a significantly importance to see and then grade epithelial damage in terms of clinical use.

There are available different types of staining techniques, the most used of them are sodium fluorescein in corneal staining, rose bengal and lissamine green in conjunctival staining [27].

1.3.4.1. The Sodium Fluorescein Staining

Corneal staining enables the evaluation of ocular surface damage by instilling a dye such as sodium fluorescein that is a vital dye because of including no intrinsic toxicity. When sodium fluorescein staining is used, staining must be graded as quickly as possible after instillation, since the dye then diffuses rapidly into the tissue and its high luminosity blurring the stain margin [27].

Sodium fluorescein dye is used with the aim of biomicroscopic observation of corneal epithelium under cobalt blue and yellow filters. The corneal fluorescein staining pattern is generally observed through a slit lamp microscopy with a cobalt blue filter. The presence of corneal epithelial defects can be observed as bright green areas (Figure 1.8.B).

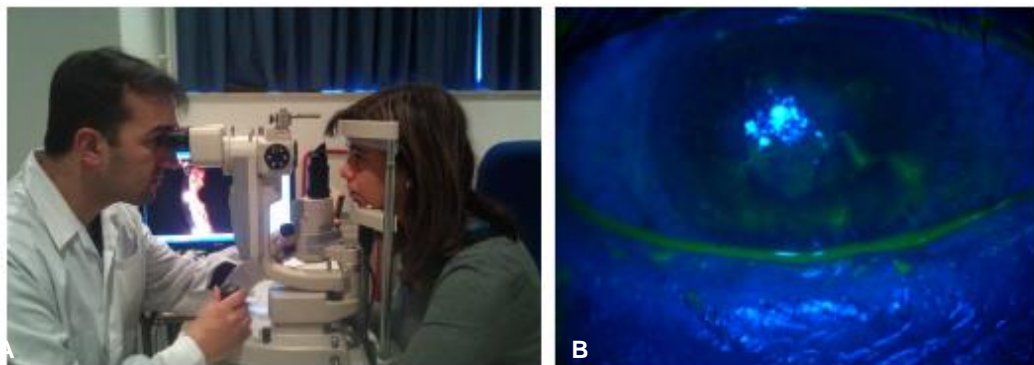


Figure 1.8 (A) Biomicroscopic examination with a slit lamp [5], (B) dryness appearance of fluorescein-stained cornea under cobalt blue filter

Strips are moistened with 0.9% sodium chloride and applied gently to the inferior fornix and then a staining pattern is observed via slit lamp microscopy. The occurred

staining pattern is graded based on the OGS. Fluorescein staining grades of greater than grade 1 are considered as abnormal [28]. If photography is delayed, it may cause blurred images, it can be seen a disadvantage of fluorescein staining.

1.3.4.2. The Rose Bengal Staining

Rose bengal has been used to assess many ocular pathologies such as meibomian gland dysfunction, superficial punctate keratitis. Past studies have shown that this staining technique is dose dependent, and light exposure can raise toxic effect on human corneal epithelial cells. This effect may explain toxicity of this dye toward bacteria and viruses. Therefore, the usage of rose bengal may make difficult the diagnosis of disease that counts on acquiring a viral culture from the ocular surface. The best results are obtained with eg. 25 μ l 1%. Because of stinging of rose bengal, instillation have the precedence by a topical anesthetic [29] (Figure 1.9).

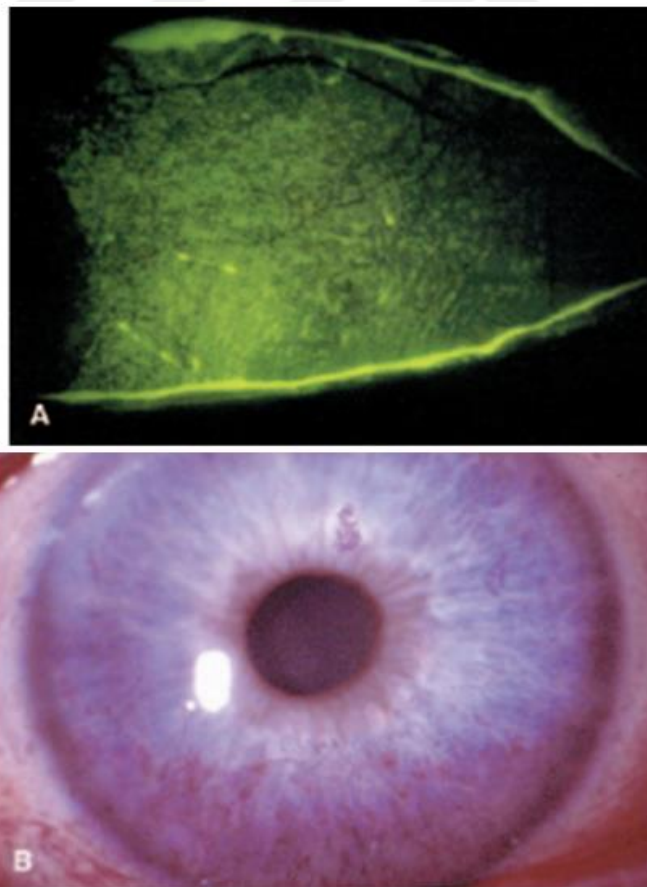


Figure 1.9 (A) Punctate fluorescein staining,
(B) assessment of rose bengal staining [29]

1.3.4.3. The Lissamine Green Staining

The lissamine green dye stains the corneal surface in a similar manner to rose bengal with its dose-dependency and visibility properties. Moreover, staining is persistent so that taking photograph need not be conducted immediately after instilling [29]. On the other hand it is in a similar manner to fluorescein since it is tolerated as fluorescein dye [29]. Lissamine green is performed with impregnated strips to drop 25 μ l 1% that will give more intense staining [29] (Figure 1.10).

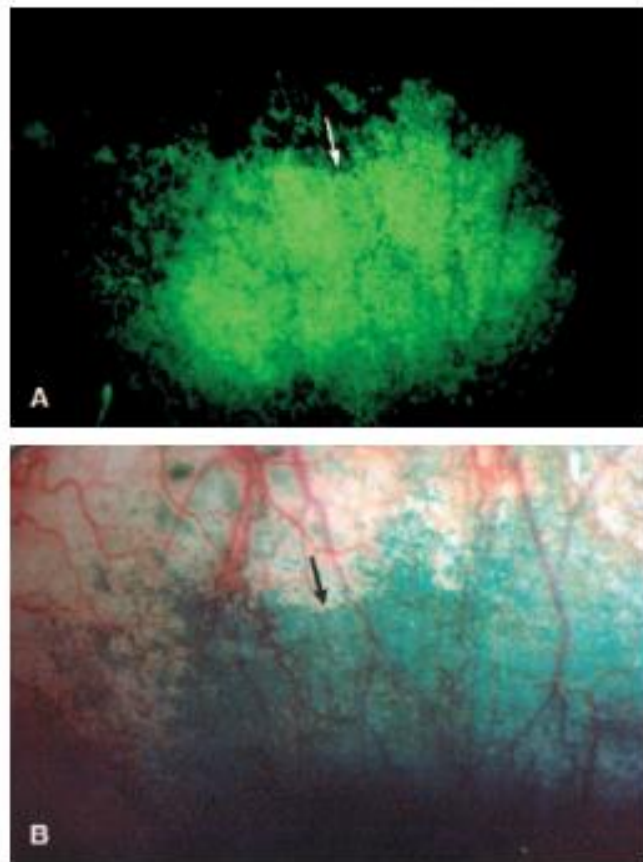


Figure 1.10 Staining of the same eye with (A) fluorescein and (B) lissamine green[29].

1.4. Oxford Grading Schema

Clinical determination of DES severity for a staining pattern is performed according to OGS. The schema is used to estimate amount of corneal surface damage in dry eye

by evaluating the staining pattern and grading based on standard charts. Staining is represented by the total numbers of punctate dots of a series of grades that range from 0 none to 5 severe (Figure 1.11).

When fluorescein staining is used, staining must be graded as quickly as possible after instillation, because of diffusion the dye rapidly into the tissue [27]. Initially, sodium fluorescein dye is instilled on the surface of dry eye. Slit-lamp is set 16 magnification with x10 oculars. The upper eyelid is lightly lifted to be able to evaluate the whole corneal surface. Unquantified instillation is a convenient approach in the clinics using the following method [29, 30]:

- A single drop of unit dose saline is instilled onto a fluorescein-impregnated strip.
- When the drop is saturated, the excess is shaken into a waste bin with a sharp flick.
- The strip is placed on the lower conjunctiva.

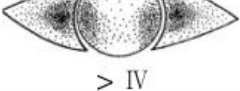
Staining appearance	Grade	Verbal descriptor
	0	Absent
	I	Minimal
	II	Mild
	III	Moderate
	IV	Marked
> IV	V	Severe

Figure 1.11 Oxford grading schema [29]

Punctate staining blurs are occurred after a short period diffusion of the fluorescein dye into the tissue. Therefore, observation and evaluation of staining rapidly are

essential in both of the right and then the left eye. If it is intended to photograph the staining pattern for grading, photography should follow immediately after each instillation [27]. If these processes are delayed, fluorescein staining may result in blurred pattern.

1.5. Related Works

An important application domain of computational skills has emerged as health care assistance with automated systems. Development of a computer based DES grading system processing dry eye images recorded by healthcare professionals and transforming into meaningful format, and so providing more efficient diagnosis tool for clinical use can be performed with advanced technology. Health care information systems can utilize this technology to ease analyzing the complex problems for humans. Taking into account that automated methods are fast, cost-effective, reusable and user-friendly, the enhancement of complicated medical diagnosis processes as an automated system would contribute significantly to clinical use for early insight of sensitive diseases. They can also be used as supporter systems in places where there may not be well-trained health care professionals.

Regarding computer-assisted implementation of clinical tests to diagnose DES, some attempts are found in the literature. There are various types of techniques used to measure DES in an objectively way. Taking into account thinner lipid layer speeds up water evaporation, the evaluation of lipid layer thickness would contribute to clinical DES analysis. For this purpose, some studies were conducted based on the lipid layer thickness measured through a sophisticated optic system [31] or an interference camera analyzing interference colors [32]. Computer-aided assessment of interference patterns of the tear film lipid layer was initially proposed in [33, 34] to diagnose DES, and then improved in [35]. CASDES, an useful computer-aided DES analysis study was implemented to give information eye practitioners by providing tear film maps depending on color-texture analysis. Texture based feature extraction; correlation based feature selection and Support Vector Machine (SVM) based classification were implemented on a tear film dataset labeled according to interference pattern.

An automatic tool to compute the BUT by analyzing tear film videos was proposed in [36]. An another automated color and texture of tear film clasification was proposed in [33], and then this study was improved for a real-time application [37]. This study indicated that the existence of multiple patterns can be evaluated as a symptom of meibomian gland abnormality, may negatively affect the classification process to be reliable due to appearing of multiple patterns.

Development of an automated grading method of fluorescein staining based on evaluation of superficial punctate keratitis was proposed in [30] on fluorescein stained corneal image dataset. OGS which is the famous one of the clinical grading techniques was selected to automate in this study. At the end of the study, it has been shown that health-care professionals may prefer to use an automated grading system depending on contribution of its use to clinical trials and their performance. In [38] automated grading of fluorescein-stained images was performed with a high accuracy on a clinical dataset, this study indicated that a clinical diagnosis tool for fluorescein staining technique can be implemented to use in real life successfully.

A recently used technique is evaluation of infrared thermography values taken from DES patients [39]. The features were extracted from Higher Order Spectra(HOS) and ranked using t-test ranking strategy. Various classifiers such as K-Nearest Neighbor (KNN), Decision Tree (DT), SVM and Naïve Bayesian Classifier (NBC) were proposed to be able to identify the dry eye and normal classes automatically with a high classification accuracy. Automated computation of the BUT test in tear film videos was aimed in [36] by detecting the blinks and analyzing the process; semi automatic calculation of the Non-Invasive Break-up Time (NIBUT) test was proposed in [40] aimed to develop a methodology for analyzing the tear stability by using video frames.

In [41] a new strategy to evaluate corneal staining: the difference of Gaussians (DoG) method to detect edges of corneal damage in collaboration with the hue saturation value (HSV) to detect colors are applied by two different specialists according to the OGS and the National Eye Institute (NEI) guidelines. This study illustrates superb correlation with the traditionally used clinical grading scales.

Segmentation of tear film images was also attempted in [42, 43]. A texture based segmentation technique was proposed in [44] to identify breakup regions of tear film by analyzing interferometry images. Segmentation process in fluorescein-stained corneal images was implemented in [45] by applying Hough transform to localise iris circular region automatically.

1.6. Aim of the Work

Technological improvements have made many aspects of data collection, management, and analysis easier and faster. There are many researchers working on different fields who rely on technology advancements in order to reduce load of their most challenging research tasks such as managing complex clinical analysis processes. Advanced image processing skills present a promising way for development more efficient diagnosis tool to use in eye clinics by healthcare professionals and the evaluation of complex biomedical image datasets in faster, cost-effective, reusable and user-friendly way. A computerized grading and diagnosis system of DES can be implemented to use efficiently in real life by utilizing these skills.

The aim of this thesis study is development of an automated OGS system to assess ocular surface and grade DES severity by processing fluorescein-stained corneal images based on the staining pattern. The computerized diagnosis system is significantly based on image processing techniques at the region of interest (ROI) level.

The proposed methodology follows to make a specific ROI definition and then region-level dry eye analysis. The dry eye spots appearing on corneal surface can be used as diagnostic indicator of DES severity. Well-trained ophthalmologists can evaluate corneal conditions at the end of a physical examination. A number of time consuming tests and examination regiments are applied to patient in order to diagnose DES in clinical settings. In addition to being time and resource intensive, current methods are also very subjective and dependent entirely on the perception of the ophthalmologists. Therefore automated, nonintrusive diagnosis techniques would greatly contribute to the clinical DES analysis. Computer-aided systems can

potentially provide more objective and reliable results which would also benefit as remote diagnosis systems in distant places where there may not be well-trained ophthalmologists and modern testing techniques. A computerized diagnosis system can be used in clinical decision making, and then can also speed up evaluation, diagnosis and treatment procedures.

1.7. Motivation

DES is one of the most common eye diseases that eye experts hear complaints about it from the eye patients. The patient's quality of life is deteriorated by DES effects significantly. The diagnosis of patients among those who have moderate to severe types of DES is very significant process, since these patients need systemic treatment. In traditional methods, evaluation of signs and symptoms of dry eye completely depends on ability and experience of ophthalmologists.

Taking into consideration that objective measurement techniques are required for diagnosis of such a common disease that increases day by day, development of a computerized diagnosis system would be helpful for decision making process of specialists in clinics. In this way, an automatic diagnosis system is provided by an user-friendly software with an easy visual interface can simplify the tasks of specialists, reduce the workload, also speed up evaluation and treatment processes. At the end of this thesis study, an automated version of OGS for a diagnosis as quick and accurate as possible of DES will be implemented to use efficiently in real life and to provide more regular and rapid improvement in symptoms and then treatment.

1.8. Outline

The paper is organized in the following manner: Chapter 2 describes briefly the data set of the fluorescein-stained corneal images employed in the conducted research and also provides detailed information regarding the methods used in this study. Chapter 3 presents the experimental study carried out in the study, the evaluation procedures used and the experimental results obtained. Finally, Chapter 4 describes the conclusions accessed from the study and some ideas intended for future work.

CHAPTER 2

MATERIAL AND METHODS

The proposed methodology in this study consists of two main steps: specific ROI definition and DES analysis at ROI-level. A ROI is a selected subset from a dataset with a special purpose. Accurate determination of the ROI has high importance for the success of the methodology due to being the initial step in the diagnosis process of DES.

Clinical assessment of DES is focused on special regions of eye, and undoubtedly a full description of the ROI with ophthalmologist's eye is a difficult task. Taking into consideration that DES diagnosis is made at the ROI level in clinical applications, automatic segmentation of the ROI would be helpful to accelerate and enhance this process. Initially computer-assisted detection of the ROI boundaries and then extraction of the ROI from whole image based on the detected boundaries can be implemented on dry eye images taken after applying sodium fluorescein staining test in clinic.

The first step is the segmentation of ROI that can be performed in two different alternatively ways: full-automatic and semi-automatic ROI definition. Full-automatic segmentation to isolate the iris region as the ROI requires a deep research for various segmentation algorithms such as Hough transform (preferred in this study), Daugman's integro-differential operator, and active contour models. The next step is processing the extracted ROI in order to enhance and prevent possible imaging errors like flash artefacts. The last step is development of automated version of clinical grading system OGS by implementing connected-component labeling (CCL) algorithm.

The flowchart of used methods in this study can be seen in Figure 2.1. Fluorescein stained corneal images taken from the patient can be interpreted with pre-processing, image processing and computational grading techniques automatically.

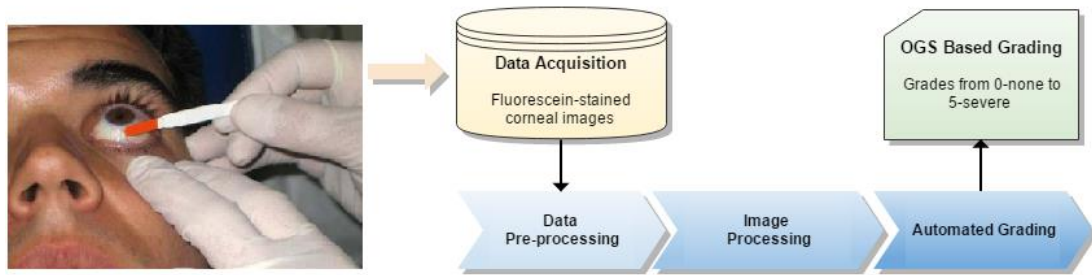


Figure 2.1 Decision making process of fluorescein stained corneal images

2.1. Data Acquisition

Data collection process of dry eye images used in this thesis study was conducted at the Keratoconus Center of Yildirim Beyazit University Atatürk Training and Research Hospital and continues for future studies. The fluorescein stained images were captured by Topcon DC-3 Integrated Camera Attachment that is a professional system for superb slit lamp photography in the year 2016 (Figure 2.2). All the images taken were exported to jpeg format with an image size of 3264×2448 pixels using post-processing software installed with the camera IMAGENet i-base and all of them were in RGB format.

The DC-3 Integrated Digital Camera Attachment is the professional system for high quality slit lamp photography, designed to work exclusively with Topcon's SL-D Series Digital Slit Lamps, the DC-3 offers 8 megapixels of resolution for clear, crisp images, videos, and multiple image capture. The DC-3 can be easily mounted into the optical path of any "D" Series Topcon Slit Lamp. All settings on the DC-3, including ISO sensitivity and image size, etc., are software driven, making image capture and manipulation extremely fast and easy [46].

The clinical image data set consists of nearly 70 data in different grades based on OGS collected from dry eye patients and labeled by an ophthalmologist (Figure 2.3.A, Figure 2.3.B). Images that have clear visibility of staining in the ROI were required and then images failing this criterion were eliminated.

Dry eye images were taken from subjects with age ranging from 25 to 70. Before data collection, subjects were asked to relax for several minutes. During data acquisition process, subjects were not allowed to blink a few seconds before photographs are taken. Some important points were specially examined before photography to eliminate participants with the following conditions:

- I.Wearing of contact lens
- II.Recent usage of tear drop or medications
- III.Current eye disease
- IV.History of serious eye disease
- V.History of ocular or facial surgery
- VI.History of general health



Figure 2.2 Topcon DC-3 digital camera used in data collection process

2.2. Extraction of Region of Interest

Regarding computer-assisted implementation of ROI selection over corneal surface to extract and focus the actual iris region with the aim of analyzing automatically, some attempts are found in the literature [47-52]: There are various techniques used to isolate ROI in an objective way. Libor and et al. implemented Hough transformation based a modified Canny algorithm on CASIA dataset to segment iris-sclera and iris-pupil boundaries with 83% success rate [50]. Petru and et al. aimed to make iris segmentation with a new method focused only red channel. A comparative study was presented among the new method, Daugmann operator and Wildes method. In iris segmentation studies, experimental studies were generally carried out on CASIA and UBIRIS iris dataset (Figure 2.3.C, Figure 2.3.D). The best performance was achieved when the suggested method was implemented on UBIRIS dataset as 92.46% [51]. In the study of Arvacheh and et al. Daugmann integro-differential operator increased the success rate to 94% on CASIA dataset [52].

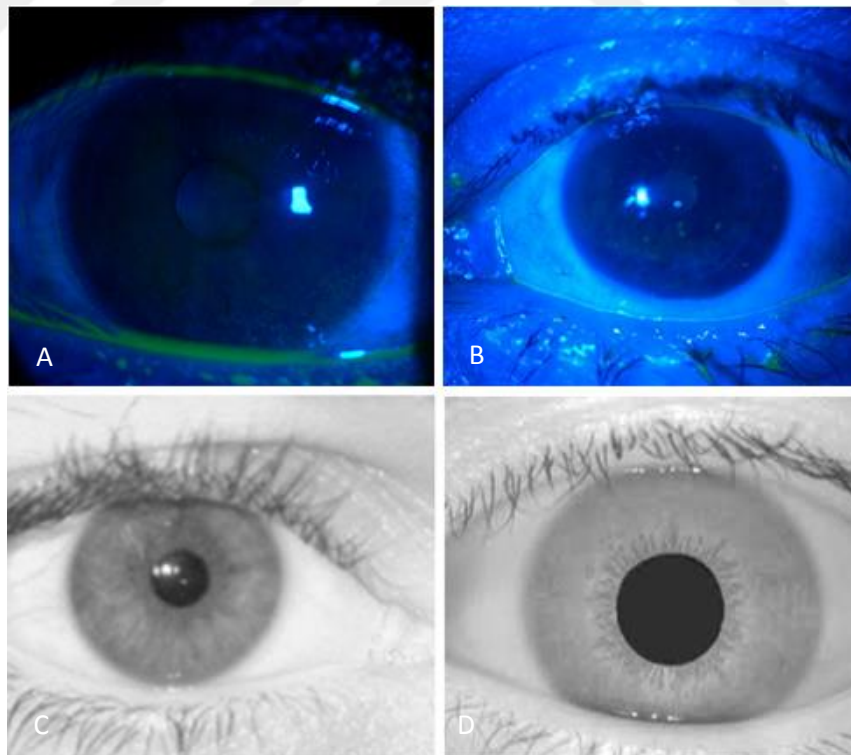


Figure 2.3 Iris samples of (A) - (B) clinical dataset; (C) UBIRIS; (D) CASIA

Iris segmentation studies in the literature generally have ideal datasets in terms of separability between iris-sclera and iris-pupil edges. However, all fluorescein-stained images may not be convenient to detect both of these boundaries exactly. Tamir and et. al. implemented RANSAC algorithm on fluorescein-stained images to segment iris [53]. In order to improve iris segmentation, the Hough transform based histogram thresholding the gamma correction method is aimed in [54]. Daugmann integro-differential operator is widely utilized for determining the position of the iris and pupil circles [55]. According to the methodology of this operator, a circular path is explored that provides maximum change in pixel values by changing the radius, central x and y position of the circular contour. To obtain precise localization, regularly decreased smoothing is implemented iteratively, and also the arcs of the upper and lower eyelids can be detected. The other important technique for iris segmentation; active contour models are utilized in [56], Ritter et al. studied for detecting the pupil boundary by working on the variance image rather than the edge image to improve performance.

2.2.1. Semi-automatic Detection of Region of Interest

The ROI can be geometrically defined as a specific area of the cornea. Before grading process, firstly segmentation of whole image and extraction of this portion is implemented. Geometric parameters such as corneal diameter and shapes may change from patient to patient. Thus, segmentation process may not be fully automated to work successfully in all cases. To prevent possible problems, semi-automatic segmentation of corneal images can be applied. Four points on the cornea region are clicked with the mouse and defined as a rectangular-shape ROI. As final part of ROI segmentation, selected region is cropped from the original image automatically and recorded for the next steps.

2.2.2. Full-automatic Detection of Region of Interest

The first step of DES grading system is to isolate the actual iris region in a digitised eye image. The iris region can be defined by two circles, first is for the iris and sclera boundary, and second is for the iris and pupil boundary, in the first. The iris circular diaphragm is placed between the cornea and the lens of the human eye whereas

the pupil circular aperture is a hole located in the center of the iris [50]. The average diameter of the iris is about 12 mm, and the pupil size can change from 10% to 80% of the iris diameter [55].

The segmentation step is important for the success of the final grading system, because if data representation has errors, grading may be resulted in poor success rates. On the other hand, segmentation process cannot be implemented easy for people who have dark pigmented irises if imaging is made under natural light.

The Circular Hough Transform (CHT) that is widely used algorithm [57] for edge detection and iris segmentation is preferred in this thesis study to make full-automatic segmentation of ROI.

2.2.2.1. Hough Transform

The Hough Transform is presented in 1962 by Paul Hough to identify features of shapes such as lines or circles [58]. The classic Hough transform, a standard computer vision algorithm used to define the parameters of geometric objects which can be especially defined in a parametrical form. A line and circle detection can be employed by regular curves in images including feature boundaries [59]. The center coordinates and the diameter of the iris can be deduced from CHT.

There are many studies implementing Hough transform based automatic segmentation algorithm to localize iris [60-63]. Most of them are generally included in iris recognition studies. The precision of the iris segmentation has a significant effect on the achieved performance of an iris recognition system. It is assumed that pupil is always central to an iris; because both pupil and iris share a central point [54]. Thus, like these assumptions may cause some mistakes in segmentation of an iris region. Eyelids and eyelashes hinder the upper and the lower regions of the iris-sclera boundary by acting as a noise, this case results in some problems during segmentation and needs pre-processing.

The steps of CHT can be seen in Figure 2.4.

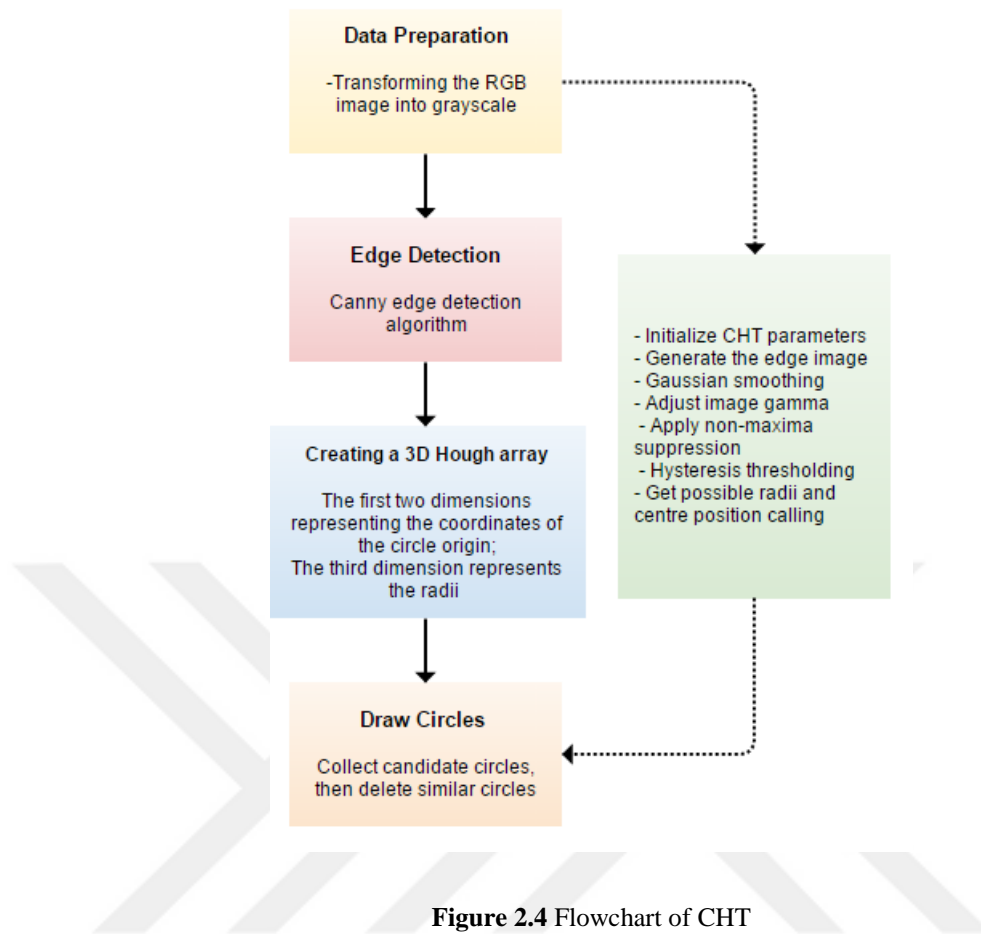


Figure 2.4 Flowchart of CHT

In Hough transform, first the edge map is generated by computing the first derivatives of intensity values in the eye image and then thresholding the result [50]. Edge map can be generated by using different edge detection algorithms. The Canny edge detector is selected in this study.

The Canny edge detection method, developed by John F. Canny in 1986, uses a multi-stage algorithm to detect a wide range of edges in images [64]. An optimal edge detector must have good detection, good localization and minimal response properties.

The steps of Canny edge detection can be given as follows [64]:

1. The image is smoothed using a Gaussian filter with a specified standard deviation, to reduce noise.

2. The local gradient and edge direction are computed at each point using different operator.
3. Apply non-maximal or critical suppression to the gradient magnitude.
4. Apply threshold to the non-maximal suppression image.

From the edge map, Hough space is viewed for parameters of the circles passing from each side point. Center coordinates X , Y and the radius r parameters can determine any circle according to the following Equation 1 [50]:

$$X^2 + Y^2 - r^2 = 0 \quad (2.1)$$

The maximum point in Hough space corresponds to center coordinates and the diameter of the most well-defined circle by the edge points.

Wildes et al. [65] bias the derivatives in the horizontal direction to detect the eyelids, and in the vertical direction to detect the outer circular boundary of the iris in edge detection step, as seen in Figure 2.5. Because the eyelids are generally horizontally aligned and also the eyelid edge map will corrupt the circular iris boundary edge map if using all gradient data. Taking only the vertical gradients for locating the iris boundary will reduce influence of the eyelids when performing CHT, and not all of the edge pixels defining the circle are needed for successful localisation. This provide circle localisation to be more accurate, and also more efficient, since there are less edge points to cast votes in the Hough space [50].

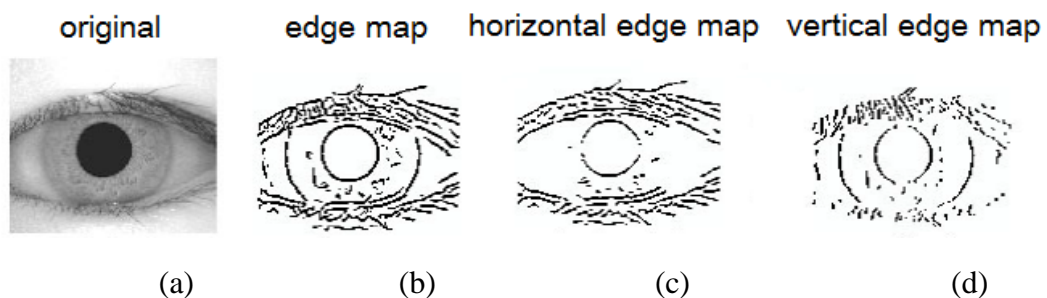


Figure 2.5. a) An eye image of the CASIA database b) corresponding edge map c) edge map with only horizontal gradients d) edge map with only vertical gradients [50]

To sum up, the Hough transform is a successful method to localize iris in an eye image [52]. It can detect the iris and pupil boundaries in circular forms and also draw eyelid edges with parabolic arcs. As for that, a binary edge map is generated with Hough method after thresholding the magnitude of image intensity gradient. As result of this, the iris boundaries can be extracted by maximizing the defined Hough transform [52].

The main advantage of the Hough transform is being tolerant to gaps in feature boundary definitions. Thus, it provides to be uninfluenced by image noise, unlike edge detector algorithms [59]. The problems with Hough transform is its requirement threshold values in edge detection, this may conclude in failure of detecting circles and critical edge points may be ignored.

2.3. Processing of ROI

The success of the grading system is significantly dependent on the quality of image dataset. Useless parts in the collected images may cause reduction of the system performance [66]. Pre-processing is applied to recover the original image if it is formerly exposed some degrading affects such as specular reflections, geometric distortion within data acquisition system, blur caused by poor optics or movement during capturing iris data; apart from, off-angle iris, faked eye images and interferences with eye images from blinks and eyelashes [66].

In clinical data acquisition process with slit lamp system, specular reflections like flash artefacts may be occurred on the iris region that can deteriorate the iris pattern and cause the misinterpreting of data. Applying pre-processing methods to exclude such artefacts as well as locating the circular iris region undoubtedly increases accuracy of the automated method. The iris images from the CASIA iris dataset do not include specular reflections thanks to the usage of near infra-red light for illumination. However, the iris images from the clinical database include specular reflections generated by imaging under natural light.

Regarding with reflection removal, this variation of illumination in images caused by the position of the artificial light source near to the subject can occur noise regions

and deform the system performance [67]. Such a reflection has high heterogeneity, as it can localize in distinct regions of the iris region in a wide range of dimensions. Such these reflection areas have intensity values close to the maximum. The extracted ROI, so image of iris part is converted to grayscale. Intensity gradients of this grayscale image are checked and in case of reflection existence these regions can be masked to improve images.

Another required method is selection of color channel so that images are modified depending on the aim of the study follows the ROI extraction step. In fluorescein stained corneal imaging under the cobalt blue filter punctate dots can be observed in green color, so the blue and red channels are discarded to extract only green channel that proceeds by applying image normalization with back ground smoothing [30]. For noise removal process, binary transformation is applied on all images. In the next step, connected regions of white pixels are detected by using a connected component detection algorithm. In this way, flash artifacts due to photography can be removed by filtering connected components that have pixels more than a pre-defined value. Finally, the remaining connected components are transferred to the grading step to be counted by the grading algorithm automatically.

To sum up, after reflection removal and elimination redundant color channels, image normalization is applied to adjust image brightness. Binary transformation is applied on all images for noise reduction and connected regions of white pixels are detected by using a connected component labeling algorithm.

2.4. Connected Component Labeling

CCL; is an algorithmic implementation of graph theory, where subsets of connected components are uniquely labeled and is used to detect connected regions in binary digital images. To implement this approach on color images in higher dimensions, they need firstly to be processed.

Extraction of dry blobs is performed on binary images obtained from thresholding phase. After the implementation, blobs can be counted, filtered, and segmented. The connected component concept is described in terms of a path, and then specification

of path based on component adjacency graph. The nature of a connected component depends on form of adjacency which one is chosen, 4- adjacency and 8-adjacency are the most common [68]. 8-adjacency is selected in the conducted study.

The component adjacency graph whose vertices represent the connected components identified locally. Next, unique labels are assigned to each of their connected components. This can be as simple as assigning to each connected component a label derived from the smallest vertex label contained in the connected component [69]. Region labeling, region extraction, blob extraction, blob discovery, connected-component analysis terms can be alternatively used for this process. In general, blob extraction is implemented on a binary image obtained from a thresholding phase. After the implementation, blobs can be counted, filtered, and segmented.

A pixel, p , at coordinates (x, y) has two horizontal and two vertical neighbors whose coordinates are given by;

- $(x+1, y)$,
- $(x-1, y)$,
- $(x, y+1)$,
- $(x, y-1)$

This set of 4-neighbors of p is indicated by $N_4(p)$ and shown in Figure 2.6.a. As seen, each pixel in this set has a unit distance from p . The four diagonal neighbors of p have coordinates are given by;

- $(x+1, y+1)$,
- $(x+1, y-1)$,
- $(x-1, y+1)$,
- $(x-1, y-1)$

This set of four diagonal neighbors of p is indicated by $N_D(p)$, Figure 2.6.b also shows these neighbors. The union of $N_4(p)$ and $N_D(p)$ forms the 8-neighbors of p , and is indicated by $N_8(p)$.

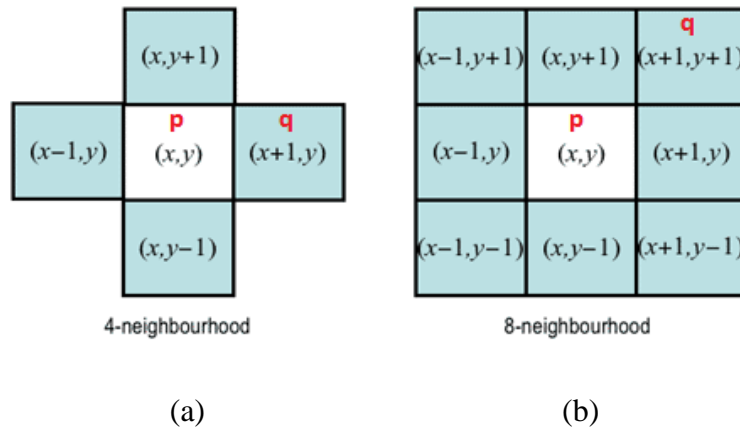


Figure 2.6 a) Pixel p and its 4-neighbors,
b) the union of 4-neighbors and diagonal neighbors of pixel p

p and q pixels are said to be 4-adjacent if $q \in N_4(p)$. Similarly, p and q are said to be 8-adjacent if $q \in N_8(p)$. Figure 2.6 indicates these concepts by coloring p and q pixels with red color. A path between pixels p_1 and p_n has a sequence of pixels $p_1, p_2, \dots, p_{n-1}, p_n$ such that p_k is adjacent to p_{k+1} , for $1 \leq k < n$ [68]. A path can be 4-connected or 8-connected based on the definition of adjacency used.

If there is available a 4-connected path between two foreground pixels p and q , they are said to be 4-connected. Similarly, if there is an available 8-connected path between them, they are said to be 8-connected. For any background pixel, p , the set of all foreground pixels connected to it is called the connected component containing p [68].

The connected component concept was just described in terms of a path, and then specification of path term depends on adjacency. The nature of a connected component depends on form of adjacency which one is chosen, 4- adjacency and 8-adjacency are the most common.

A small binary image with 4-connected components is shown in Figure 2.7 (a). It can be clearly seen that in Figure 2.7 (b), selecting 8-adjacency can reduce the number of connected components of two [68].

The pixels in each different connected component are assigned a unique integer, from 1 to the total count of connected components. The pixels labeled 1 belong to the first connected component; the pixels labeled 2 belong to the second connected component; and so on. On the other hand, background pixels are labeled 0. Figure 2.7 (c) shows the label matrix corresponding to Figure 2.7 (a), Figure 2.7 (d) shows the label matrix corresponding to Figure 2.7 (b). Then the row and column indices for all the pixels belonging to which object [68].

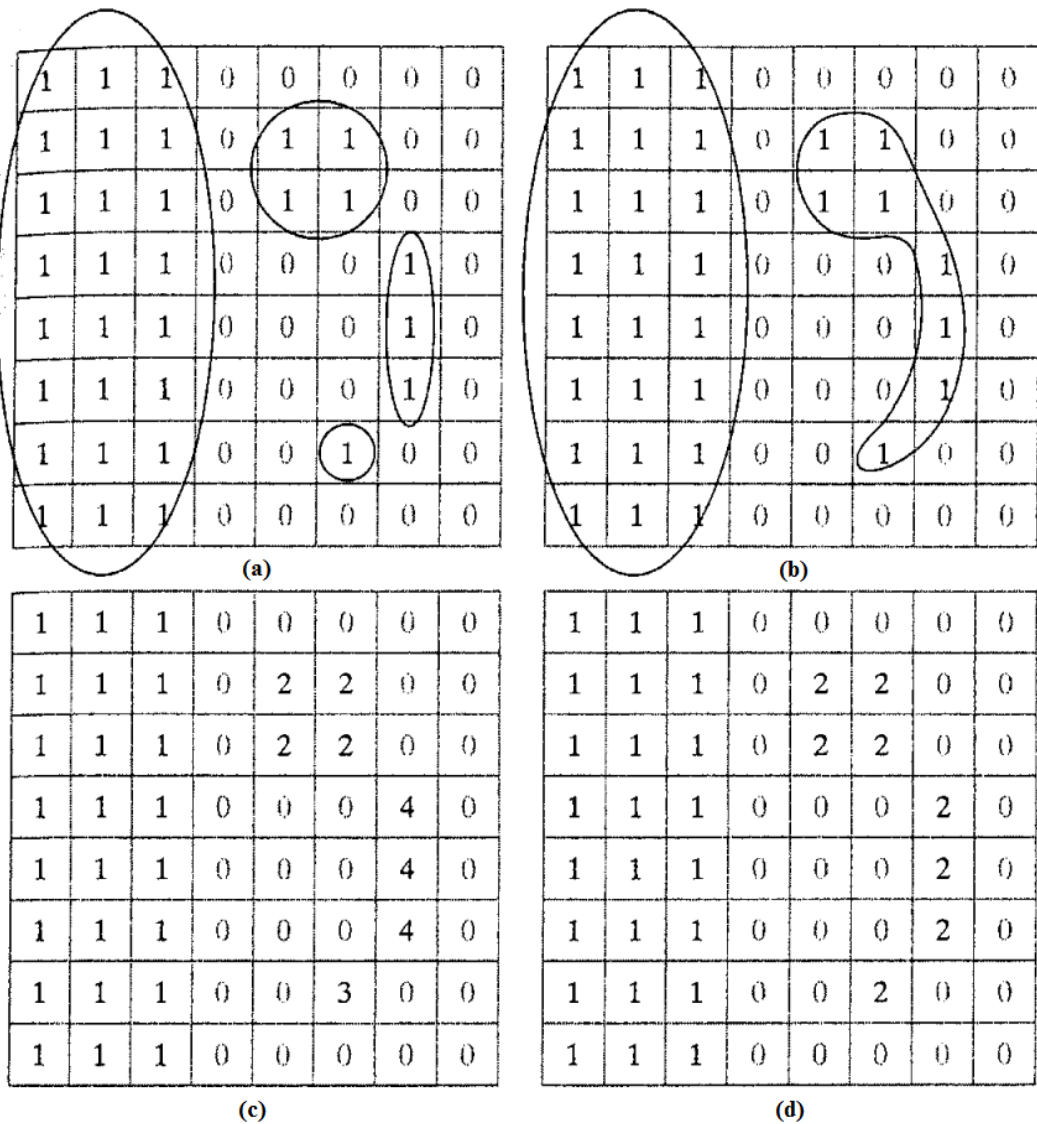


Figure 2.7 Connected components **a)** four 4-connected components. **b)** two 8-connected components. **c)** label matrix obtained using 4-connectivity **d)** label matrix obtained using 8-connectivity.

2.5. Statistical Methods

The pairwise correlations among the ophthalmologist and automated system can be determined using Pearson's correlation coefficient as follows:

$$r = \frac{\sum XY - \frac{(\sum X)(\sum Y)}{n}}{\sqrt{\left(\sum X^2 - \frac{(\sum X)^2}{n}\right) \left(\sum Y^2 - \frac{(\sum Y)^2}{n}\right)}} \quad (2.2)$$

Pearson's correlation coefficient gives information about correlation, but it is not related with agreement. The agreement of the predicted DES grading and the traditional clinical grading conducted by the ophthalmologist is determined using Lin's Concordance Correlation Coefficient (CCC) [70]. Bland-Altman [71] analysis supports these coefficients.

The primary analysis is a comparison of the ophthalmologist-graded score to the automated-graded score.

Linear regression analysis is used to generate an predictor of DES grade. The relationship between graded score by the ophthalmologist and the automatically graded score is derived according to the obtained linear regression fit. The best approach to the clinically graded score may be written as follows according to Linear regression analysis:

$$G_{pred} = C1 \log(N_{dots}) + C, \quad (2.3)$$

G_{pred} represents the automatically predicted DES grade and N_{dots} represents the number of punctate dots.

CHAPTER 3

IMPLEMENTATION

In the data acquisition process of this study, sodium fluorescein staining was applied on DES patients during clinical evaluation. Fluorescein-stained corneal images were gathered via slit lamp photography after instillation of sodium fluorescein solution into the conjunctival tissues of both eyes of each subject.

In the implementation part of this study, a computerized DES diagnosis system was implemented at the ROI level by applying computational methods on digital fluorescein-stained corneal images. In analysing and grading of these digital images image processing skills were substantially required.

The first step of the study is the segmentation of the digital images and extraction of ROI from the remainder of the image. The user of the developed computer-assisted system firstly defines the ROI. This process can be performed in two different alternatively ways: In first, the ROI is selected as a geometrically defined area of the cornea. This is useful for usage by ophthalmologists since they are primarily focused on inferior cornea region in clinical examination. In second, iris part is full-automatically detected and extracted from the whole fluorescein-stained corneal image to consider as the ROI. Then, the image is automatically cropped based on the selected ROI and processed to obtain ideal version. The next step; CCL; is detecting individual dry areas by analyzing which pixels are connected to each other. Each group of connected pixels, so each dry area are given a label to identify it so that each can be distinguished from the others, so we can make measurements of dry regions separately. To visually show the user the distinct dry regions, a different color is assigned each region and the boundaries of them are drawn. The total count of all dry areas and mean intensity, size of the area, perimeter, centroid, diameter information of each dry area are reported at the end of computational methods. According to the presented list of the dry blobs at final, it can be said that the ophthalmologists can see a detailed quantitative analysis of dryness and severity of

DES graded according to automated OGS by analyzing measurements of dry punctate dots.

Flowchart of the implemented study can be seen in Figure 3.1.

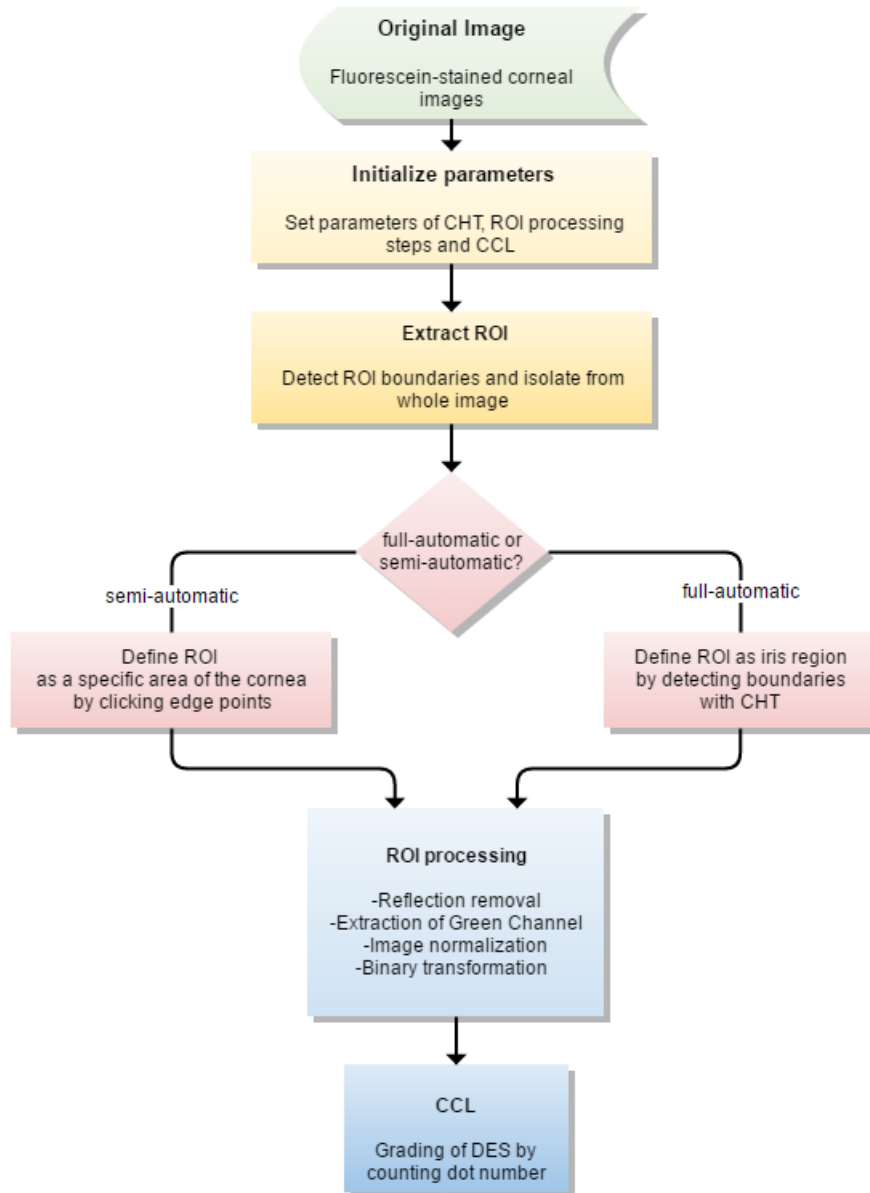


Figure 3.1 Flowchart of the implemented study

3.1. Conduct of Staining

Sodium fluorescein staining that is widely used technique by ophthalmologists in clinical evaluation was selected in this study and applied to patients during data collection process. In clinical evaluation, sodium fluorescein dye is instilled on the surface of dry eye initially. Slit-lamp is set 16 magnification with x10 oculars. The upper eyelid is lightly lifted to be able to evaluate the whole corneal surface.

Punctate staining blurs are occurred after a short period diffusion of the fluorescein dye rapidly into the tissue. Therefore, observation and evaluation staining rapidly are essential in both of the right and then the left eye.

During data collection process, photography followed immediately after each instillation. If these processes are delayed, fluorescein staining may result in blurred pattern. Images that have clear visibility of punctate staining in the ROI were required, then images failing this criterion were eliminated (Figure 3.2). Unfortunately, some images were eliminated with this reason.

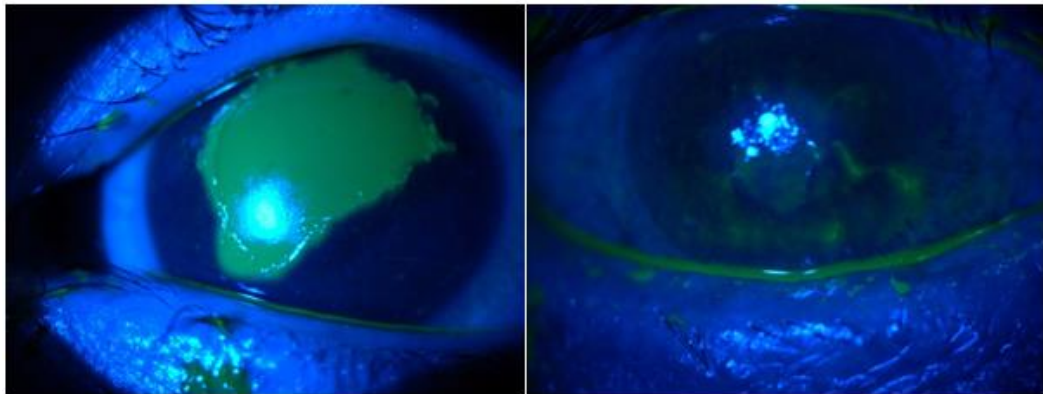


Figure 3.2 Eliminated samples of dataset because of having an another epithelium defect

3.2. Image Capture Technique

The data set used in the study is an original data set that has fluorescein-stained corneal images taken from nearly 70 dry eye patients via slit-lamp photography by an ophthalmologist. In clinical evaluation, staining is graded right after instillation of sodium fluorescein solution into eyes of patients. To guarantee proper distribution of

the dye throughout the tear film surface, the subject blinks several times. Then, the specialist does not apply any cleaning processes before taking of corneal images because residence time of dye shows impact of fluorescence. Photography initially centers on the lower cornea region because it highly keeps dye in DES [20], and then corneal images including also superior region were taken. These images were recorded by Topcon DC-3 Integrated Camera Attachment that is a professional system for superb slit lamp photography in the year 2016, images were placed 50 cm away from chin-rest. All the images taken were exported to jpeg format with an image size of 3264×2448 pixels using post-processing software installed with the camera IMAGEnet i-base and all of them were in RGB format. Cobalt blue filter provided clear visibility of occurred dry regions. Camera parameters were fixed for all subjects.

3.3. Clinical Grading

After data collection process was completed, all images were traditionally labeled according to the OGS currently used by ophthalmologists in clinics. This system uses a 0-none to 5-severe grading scale depending on existence and intensity of dry areas (Figure 3.3). Clinical grading system firstly focused on inferior region to diagnose DES. At the end of study, an comparison of clinical grading system and computerized grading system was presented.

3.4. Selection of Region of Interest

Analysis and grading processes of DES were conducted at the ROI level. After data collection, the first step of the experimental study is the selection and extraction of the ROI part from the whole fluorescein-stained corneal image. The implemented study provides ROI selection in two different ways; first is user defined semi-automatic ROI selection, second is full-automatic ROI selection.

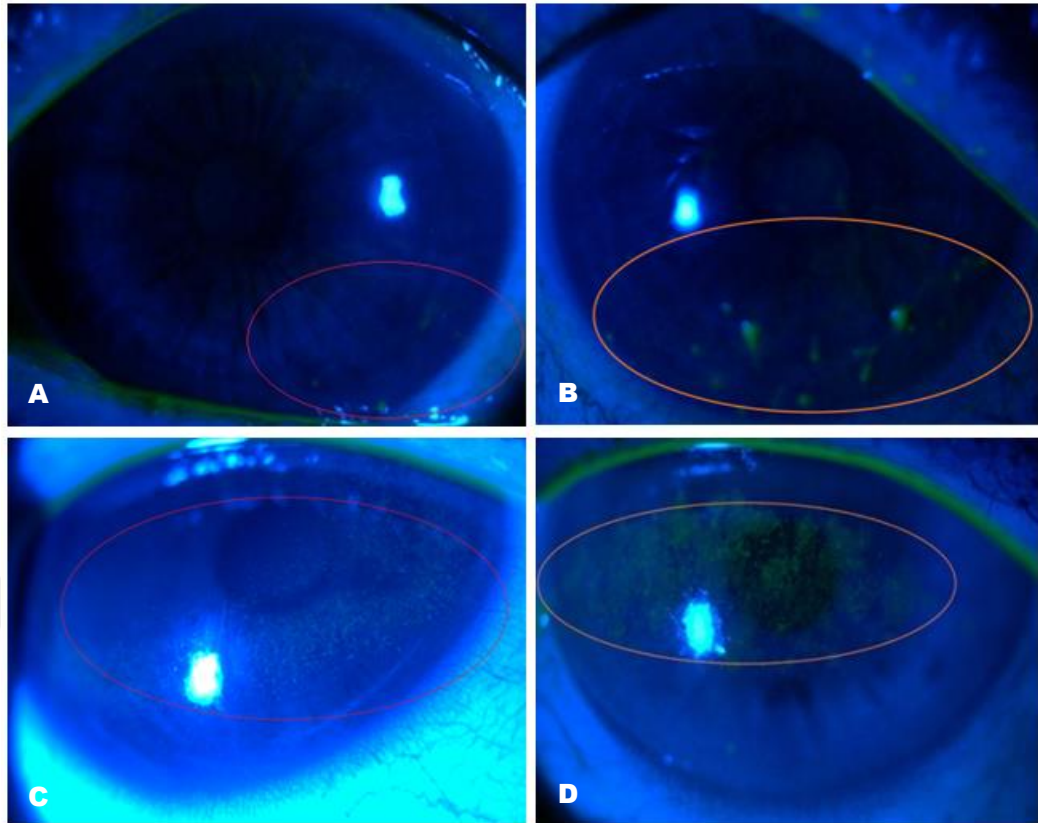


Figure 3.3 Grading of staining patterns, (A) grade:1, (B) grade:2, (C) grade:3, (D) grade:3

Geometric parameters such as corneal diameter, eyelid shape could have variations among patients, therefore segmentation step may not be exactly automated in an easily way. On the other hand, ophthalmologists have preferred to focus on directly inferior cornea region of eye in clinical grading. Therefore, this study primarily provide user defined ROI selection semi-automatically so that four edge points are selected as corners of a rectangular ROI manually by the program user and cropped from the original image automatically.

In another way, boundary of iris region can be detected and this region can be extracted as ROI full-automatically. The success of automatic segmentation step is significantly dependent on the quality of image dataset that was observed by applying on clinical dataset samples and several CASIA samples also.

In this step, studies were conducted to obtain the best segmentation minimizing possible errors that may be occurred in ROI determination with eye by

ophthalmologists in clinical grading and diagnosis. Therefore, the first step; determination of ROI has primary importance in terms of success of the study.

3.4.1. Semi-automatic Detection of Region of Interest

DES diagnosis tool provides semi-automatic selection of ROI by selecting user defined ROI option. Semi-automatic means that the program user manually selects a rectangular region wherever is needed to analyze in detail as ROI by clicking four points along the edge of the related region on the whole image, and then extraction of the selected area as ROI is performed automatically. In this way, the first step that is clicking on four different points with cursor prevents to conduct full-automatic segmentation of the ROI.

See Figure 3.4 for implementation of semi-automatic ROI selection on an image. The ROI is selected as a geometrically defined area of the cornea. This segmentation type is useful for use of ophthalmologists since they are primarily focused on specific regions in clinical examination.

3.4.2. Full-automatic Detection of Region of Interest

A segmentation algorithm involves two procedures: iris localization and noise reduction. The iris localization process takes detection of boundary between the sclera and iris, the noise reduction process refers to localizing the iris from the noise (non-iris parts) in the image. These noises include the sclera and artifacts.

DES diagnosis tool provides full-automatic selection of ROI by selecting automated ROI option. Full-automatic means that the program user selects a fluorescein-stained image, and then iris region is full-automatically detected and isolated from the remainder of the image to consider as the ROI by the program. Then, the image is automatically cropped based on the ROI and iris part is extracted. Thanks to this, unnecessary parts of image are discarded and program ignore negligible areas, also ophthalmologists can focus on only primary regions to analyze DES in more easily way. The success of automatic segmentation step is significantly dependent on the quality of image dataset that is observed by applying on several CASIA samples also (Figure 3.5).

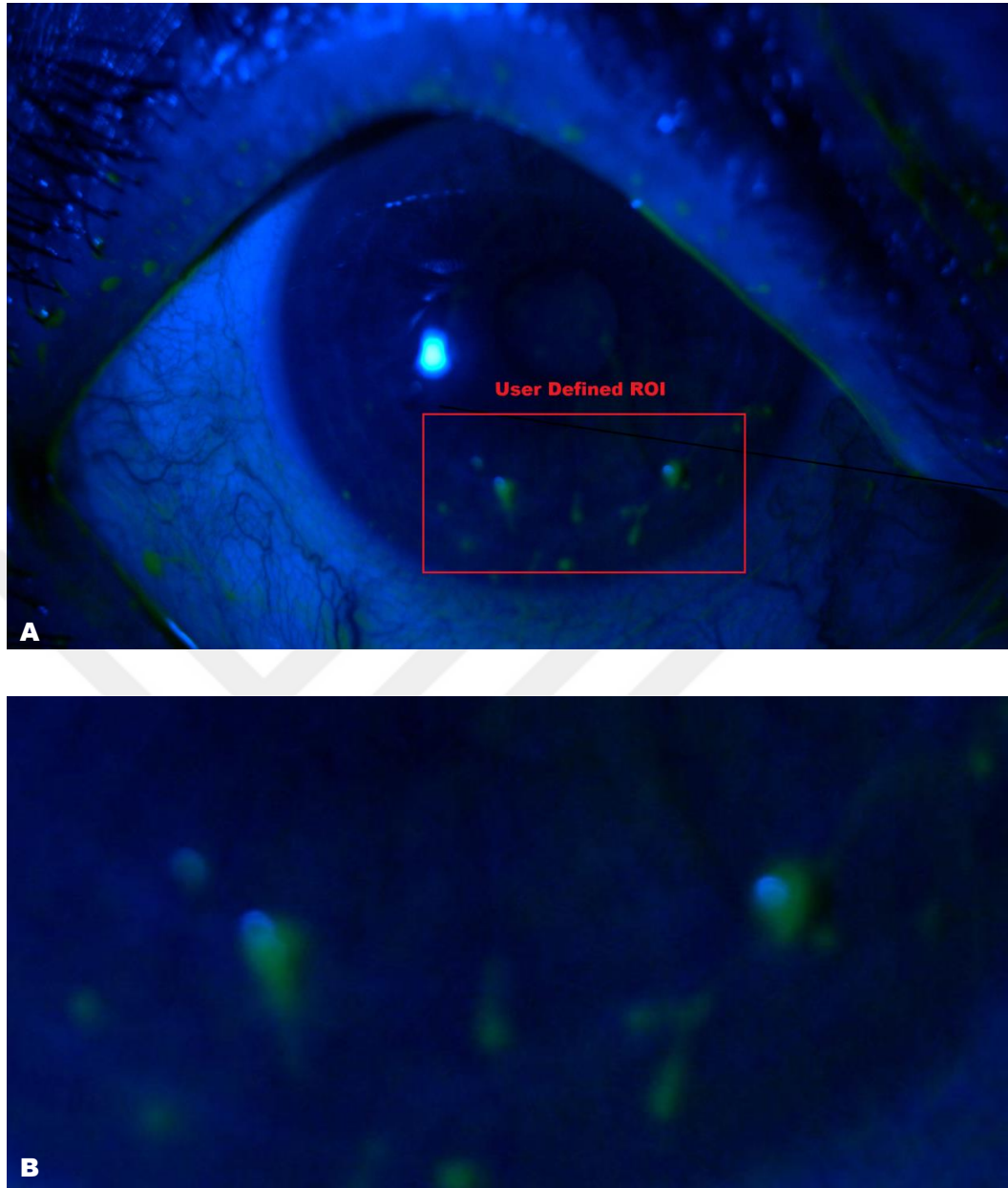


Figure 3.4 (A) Digital image of the fluorescein-stained cornea under cobalt blue filter, user selects a region as ROI by clicking four points, (B) cropping of the selected ROI

The CHT is implemented to detect where the iris boundaries are placed on image with iris detector function (Table 3.1). The module of the program searches and returns the centre coordinates and radius of the detected iris boundary on the image by implementing the CHT and Canny edge detection to create the edge map.

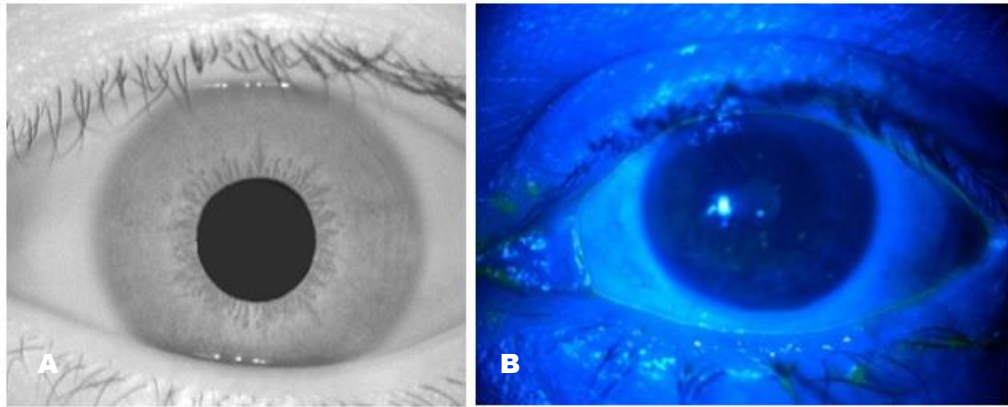


Figure 3.5 (A) An image of CASIA dataset, (B) an image of clinical dataset

Table 3.1. Arguments of iris detector module and their values

Arguments of Iris Detector Function			
Lower iris Radius to search for:	80	Hithres: threshold for creating edge map	0.20
Upper iris Radius to search for:	150	Lowthres: threshold for connected edges	0.19
Scaling: scaling factor for speeding up the Hough transform	0.4	Vert: vertical edge contribution (0-1)	1.00
Sigma: amount of Gaussian smoothing to apply for creating edge map.	2	Horz: horizontal edge contribution (0-1)	0.00

The Canny edge detection algorithm is firstly applied for generating edge map of the image. Sigma - standard deviation of Gaussian smoothing filter, scaling – factor to reduce input image by, vert - weighting for vertical gradients, horz - weighting for horizontal gradients inputs are given the iris detector algorithm and gradient - edge strength image (gradient amplitude), orientation image outputs are obtained. Then, image gamma is adjusted to enhance contrast in dark regions. The result image, orientation image and radius inputs are given a non-maxima suppression function. This function is used for performing non-maxima suppression on an image using the

orientation image. It is assumed that the orientation image gives feature normal orientation angles in degrees (0-180). The radius information is distance in pixel units to be looked at on each side of each pixel when determining whether it is a local maxima or not. It uses bilinear interpolation to estimate intensity values at ideal, real-valued pixel locations on each side of pixels to determine if they are local maxima. See Figure 3.6 for implementation of Canny edge detection algorithm on the fluorescein-stained image.

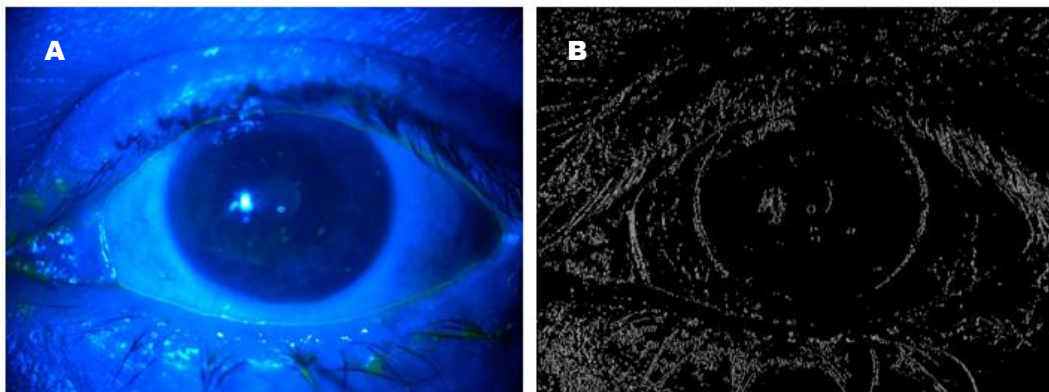


Figure 3.6 (A) An eye image from the clinical dataset, (B) corresponding edge map

See Figure 3.7 for implementation of Canny edge detection algorithm on the sample of well-known CASIA dataset.

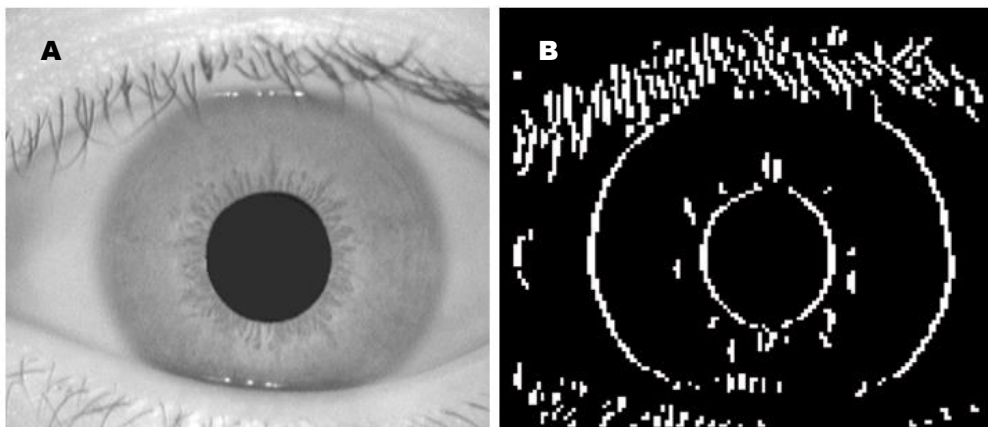


Figure 3.7 (A) An eye image from the CASIA database (B) corresponding edge map

The range of radius values are determined based on the properties of gathered images for the clinical data set. For the samples from the CASIA dataset, diameter of the iris

is determined to be in the range of 90-150 pixel, pupil diameter is determined to be in the range of 28-75 pixels according to literature information [54]. To improve iris detection process in more efficient and accurate way, Hough transform initially finds edge between iris and sclera, and then edge between iris and pupil in the formerly detected iris region. After this operation, information of radius and center coordinates of both edges are obtained and stored. Lastly hough transform is applied on the edge image and iris boundaries can be obtained.

In conducted study, successful segmentation of both iris and pupil boundaries is achieved on ideal image samples of CASIA data set. In these samples, accurately determination of iris-sclera and iris-pupil boundaries can be seen in Figure 3.8.

It is experimented that pupil detection process is not sufficiently successful when clinic data set including fluorescein-stained corneal images is used. On the other hand, only the detection of iris and sclera boundary is needed to define ROI for clinical data set. In addition, segmentation success can be increased by improving photographing technique by ophthalmologists. In fluorescein-stained image iris-sclera boundaries can be detected accurately and iris region is extracted as ROI as in Figure 3.9.

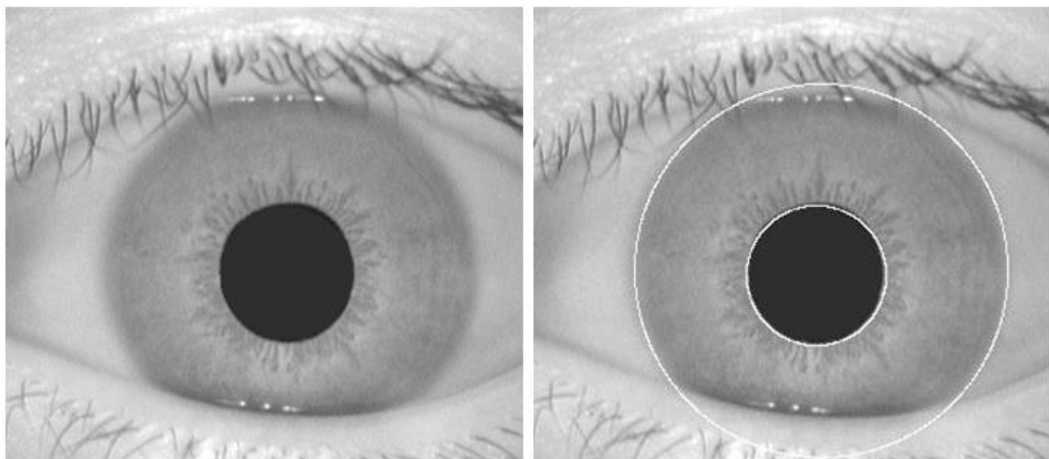


Figure 3.8 Automatic detecting iris and pupil boundaries (white circles) on a CASIA image

Automatic dry area detection is performed on directly iris region since it has already defined and used as ROI in clinical applications. In this case, the remaining parts of

eye must be ignored by program also. So, a masking application is formed to mask the remaining corneal surface and iris region is extracted as seen in Figure 3.10.

Specular light reflections can occur within the iris region corrupting the iris pattern and hence a technique is required to isolate and exclude these artifacts as well as locating the circular iris region (Figure 3.11).

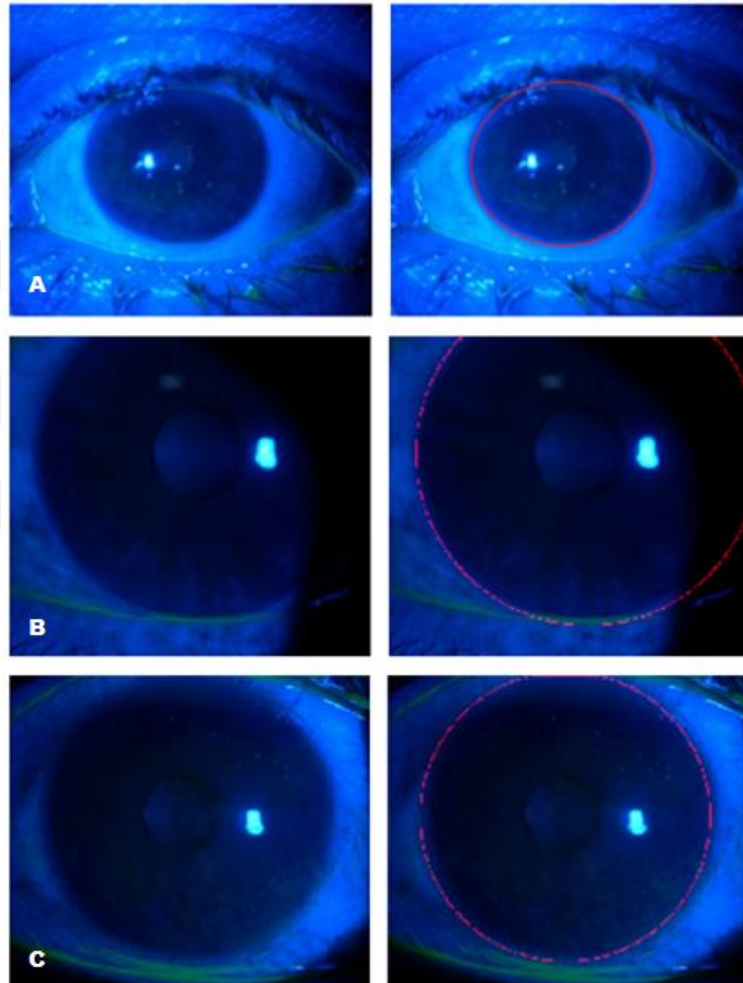


Figure 3.9 Automatic detection of iris boundaries (red circle) on clinical dataset, A, B, C, D, E, F are successful segmentation; G, H are unsuccessful segmentation

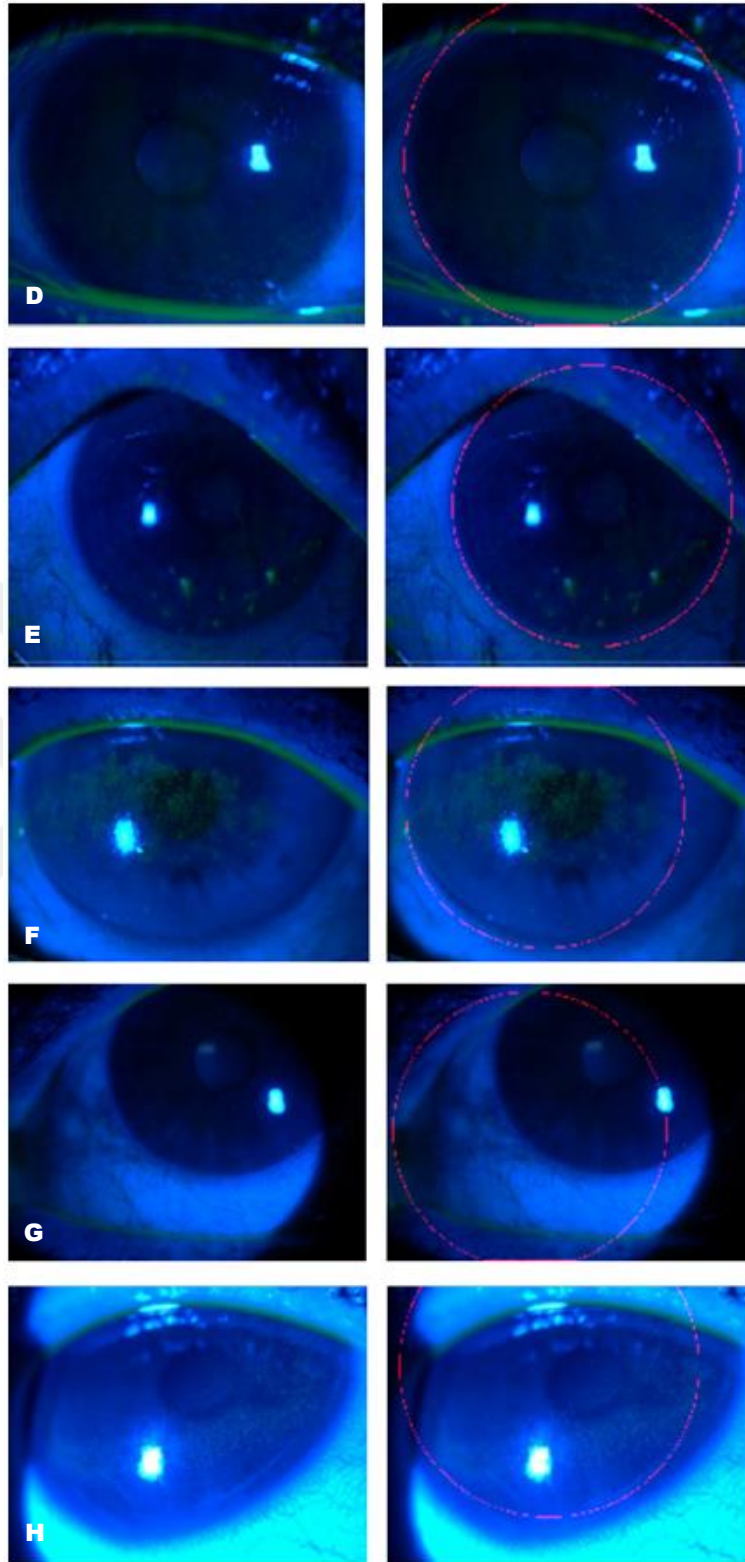


Figure 3.9 Automatic detection of iris boundaries (red circle) on clinical dataset, A, B, C, D, E, F are successful segmentation; G, H are unsuccessful segmentation

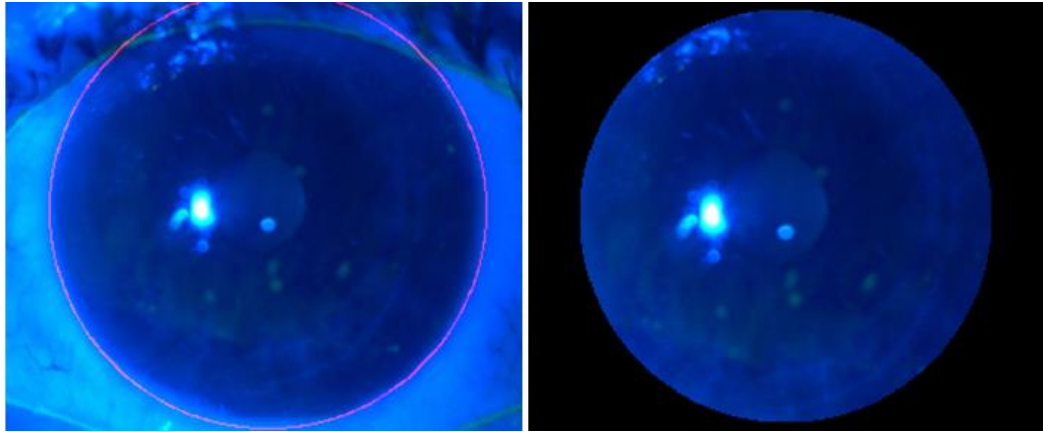


Figure 3.10 Automatic cropping ROI on an image of clinical dataset

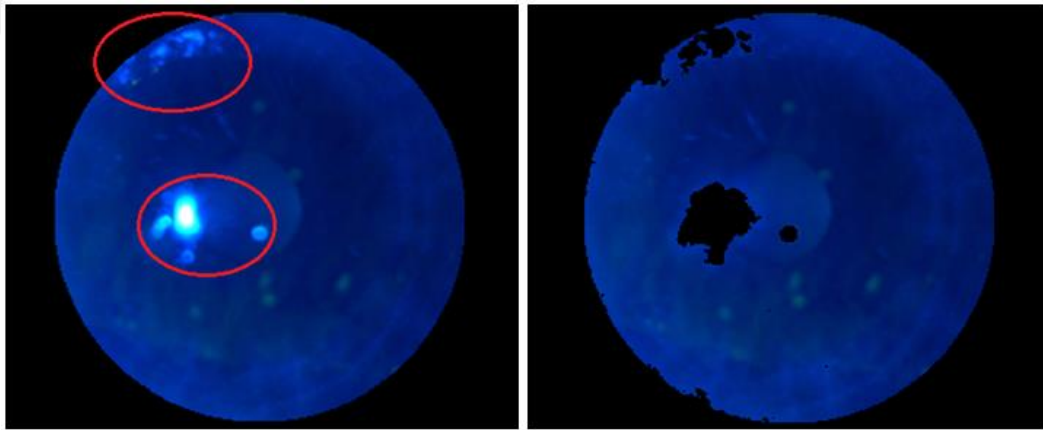


Figure 3.11 Removing specular flash artifacts occurred within the iris region

3.5. Automated Oxford Grading Schema

After the initial segmentation and noise removal process to extract the ROI accurately, the color channels except green are discarded (Figure 3.12.A). Next, gray scale transformation and normalization with back ground smoothing processes are conducted (Figure 3.12.B). By thresholding the images, punctate dots are highly detected.

After normalization process, the images are transformed to binary image format to eliminate noise in the image. Then a blob detection algorithm is required to detect dry areas. The CCL algorithm implemented on white pixels to filter. After the

connected dry areas of white color are filtered, the blobs are counted to acquire the punctate dot number.

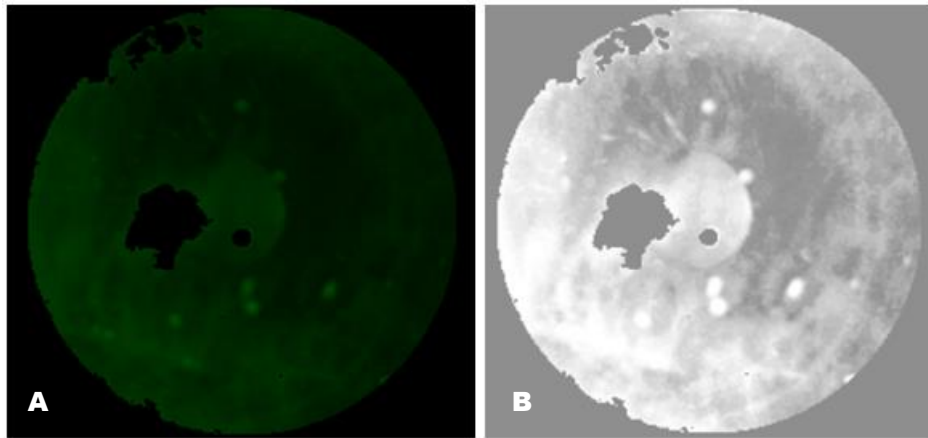


Figure 3.12 (A) Extracting green channel, (B) transforming rgb to gray, background normalization

Detected punctate dots that can be indicator of DES according to OGS are marked in red dots. Detected bigger areas than a predefined threshold value can be indicator of filamentary keratitis disease that is a condition in which strands (“filaments”) composed of degenerated epithelial cells and mucus develop on and adhere to the corneal surface causing pain. These areas are not considered as punctate dots and marked in blue crosses. Grading details of Figure 3.13 and Figure 3.14 can be seen in Table 3.2 and Table 3.3 orderly.

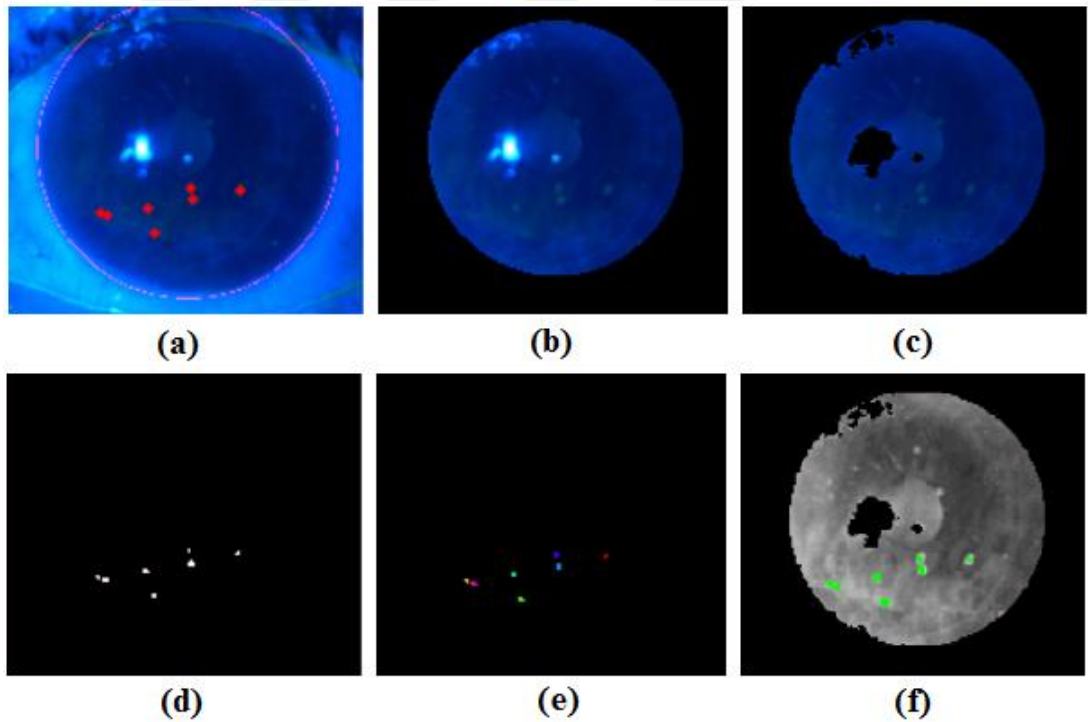
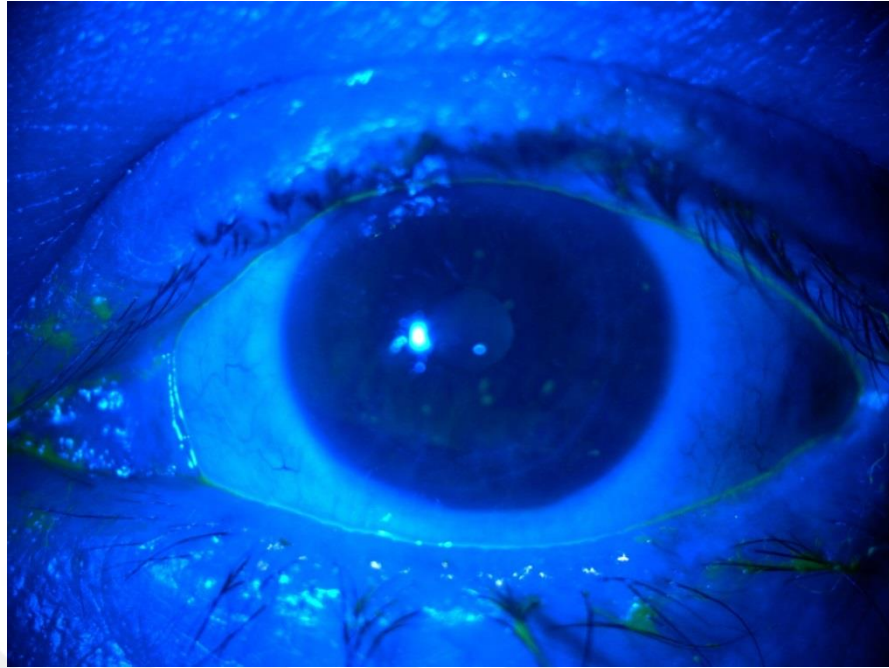
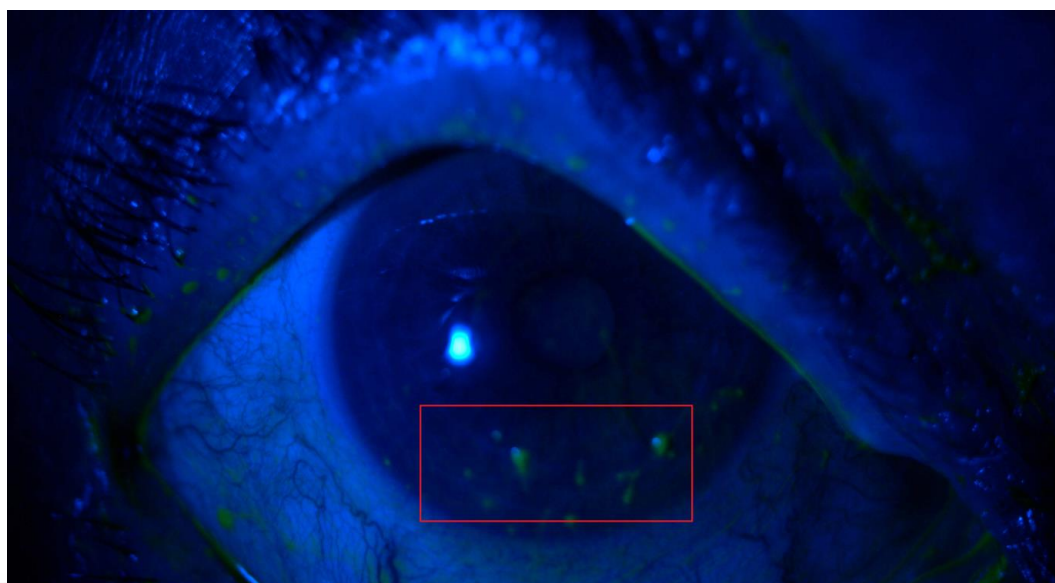


Figure 3.13 (a) Detection of iris boundaries as ROI full-automatically (red circle). (b) extraction of ROI (c) reflection removal (d) binary image after pre-processing the image (extraction of the green channel, image normalization with background smoothing, thresholding) (e) identifying individual dry areas by seeing which pixels are connected to each other and assigning each distinct dry area a different color (d) determining the borders of all the dry areas (f) counting of punctate dot number.



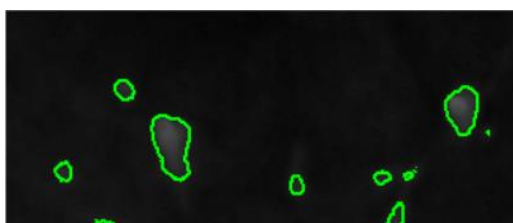
(a)



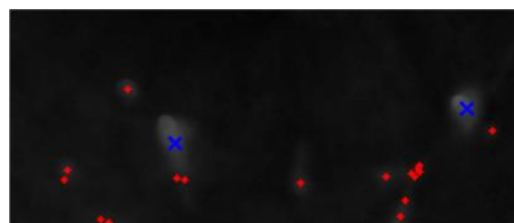
(b)



(c)



(d)



(e)

Figure 3.14 (a) Cropping of the digital image of the inferior cornea based on the ROI defined semi-automatically (red circle). (b) binary image after pre-processing the image (extraction of the green channel, image normalization with background smoothing, thresholding) (c) identifying individual dry areas by seeing which pixels are connected to each other and assigning each distinct dry area a different color (d) determining the borders of all the dry areas (e) counting of punctate dot number.

Table 3.2. Quantative analysis results of each dry blob reported at the end of computational methods in Figure 3.13 and grading as grade 1

Blob #	Mean Intensity	Area	Perimeter	Centroid		Diameter
1	0.8	9.0	8.8	84.7	188.4	3.4
2	0.9	18.0	13.1	91.3	190.9	4.8
3	0.9	18.0	13.1	126.7	183.1	4.8
4	0.8	14.0	11.7	133.8	205.4	4.2
5	0.8	9.0	8.8	165.7	165.4	3.4
6	0.9	22.0	15.7	168.0	176.5	5.3
7	0.8	10.0	8.8	209.5	167.0	3.6

Table 3.3. Quantative analysis results of each dry blob reported at the end of computational methods in Figure 3.14 and grading as grade 2

Blob Number	Mean Intensity	Area	Perimeter	Centroid		Diameter
1	34.3	510.0	89.0	86.9	238.1	25.5
2	30.0	3.0	4.0	82.0	253.0	2.0
3	30.1	10.0	14.2	135.6	310.7	3.6
4	31.8	258.0	91.7	147.8	316.7	18.1
5	37.3	623.0	96.9	175.9	118.2	28.2
6	46.9	3954.0	301.3	246.3	198.8	71.0
7	30.0	1.0	0.0	249.0	249.0	1.1
8	30.0	3.0	3.4	258.7	252.7	2.0
9	33.9	434.0	85.0	431.4	257.9	23.5
10	33.0	333.0	82.7	557.4	246.8	20.6
11	35.6	627.0	115.5	578.7	305.5	28.3
12	30.2	6.0	7.4	584.8	283.3	2.8
13	30.7	93.0	45.0	596.0	243.8	10.9
14	30.0	6.0	6.0	599.0	247.5	2.8
15	30.0	6.0	6.0	604.5	237.0	2.8
16	30.0	4.0	4.8	607.5	240.0	2.3
17	31.0	1.0	0.0	608.0	232.0	1.1
18	48.9	2507.0	203.9	676.2	147.3	56.5
19	30.1	19.0	19.9	714.1	180.6	4.9

More samples in different DES severities and their grading details are given in Appendix A and Appendix B.

CHAPTER 4

RESULTS

In this study, an automated grading and diagnosis system for evaluation of DES is implemented to use efficiently in real life; it became possible to access more quantitative analysis than clinical evaluation. The implemented study also avoids the errors that might be caused by specialists' heavy workload; also it helps the specialists in evaluations that require attention. By using this system, the severity of the corneal surface damage can be predicted before an operation. Thus, the specialist can decide if the operation is convenient or not for the related patient. Moreover, treatment procedures can be conducted based on more objective grading results. The data set used in this experimental study continues to grow for future studies. Experiments still continue and are improved as new data is obtained.

Fluorescein staining method is represented by punctate dots that are ordered on a log scale. It has been previously known that OGS has a logarithmic progress; so clinical grade and the detected dot number have a logarithmic relationship. In Figure 4.1, the clinical staining score assigned by the ophthalmologist is plotted versus the automatically calculated number of dots, logarithmic scale of N_{dots} that has actually no limit, however; any image including N_{dots} greater than approximately 1000 have not been seen; that is, $\log(N_{dots})=3$. Furthermore, Bland-Altman analysis of clinical grading and automated grading is given in Figure 4.2.

According to Equation 3, linear regression analysis of clinical grading and the number of automatically detected dots shows that $C1 = 1.3244$, $C2 = 0.0612$. As a result, DES grade of any fluorescein-stained corneal image can be predicted from the following formula as:

$$G_{pred} = 1.3244 \log (N_{dots}) - 0.0612 \quad (\text{for } N_{dots} > 0),$$

$$G_{pred} = 0 \quad \text{for } N_{dots} = 0.$$

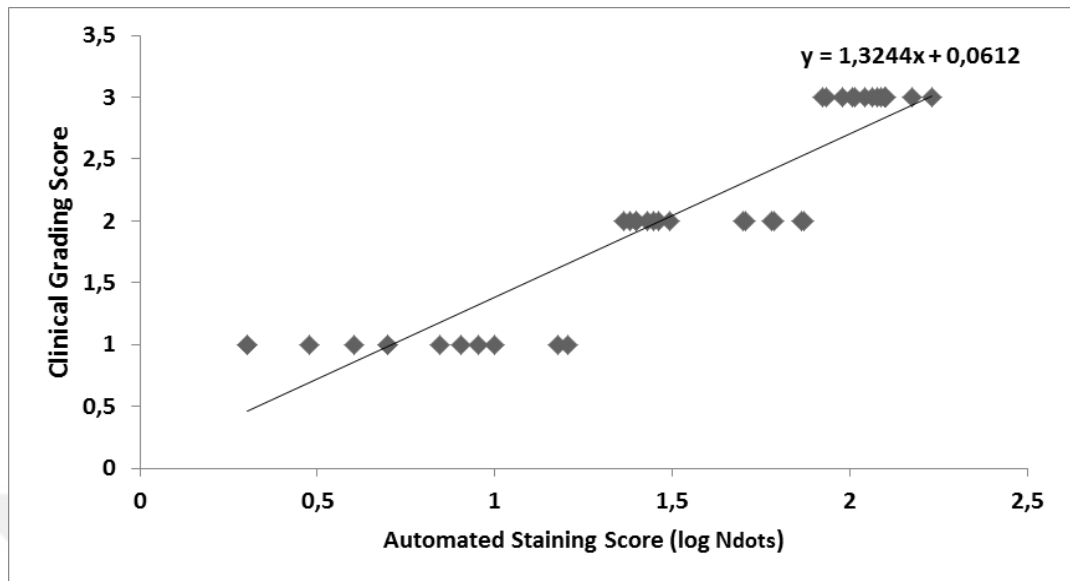


Figure 4.1 Individual clinical staining scores for all 70 images versus automatically detected punctate dot number (N_{dots}); per linear regression $G_{pred} = 1.3244 \log(N_{dots}) - 0.0612$.

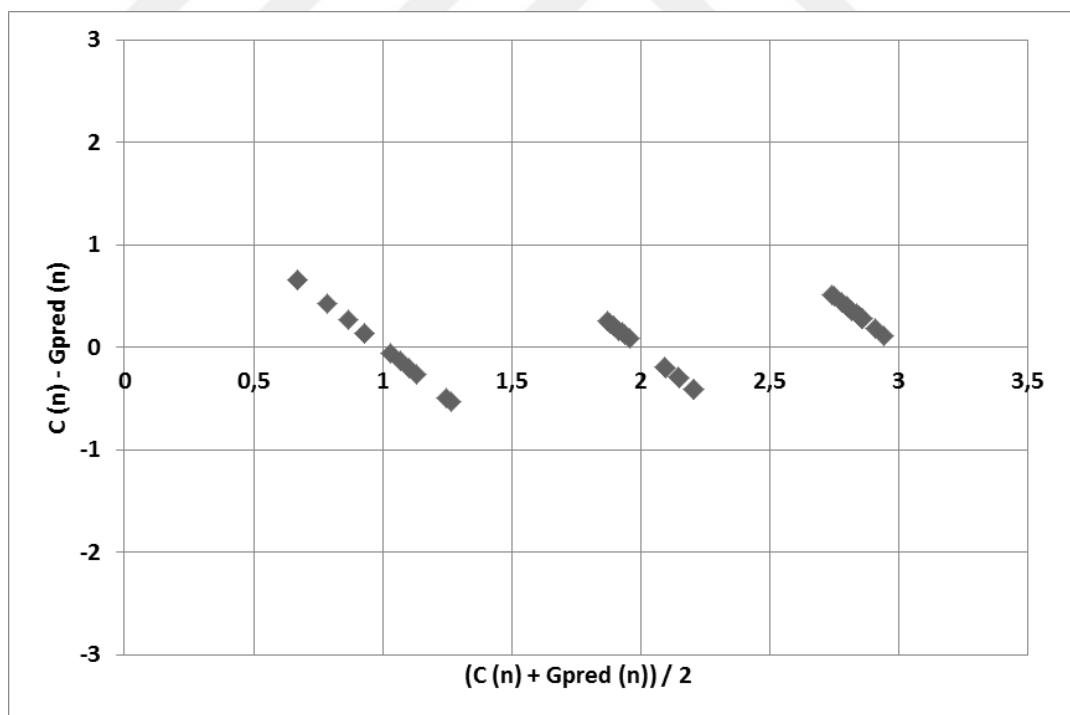


Figure 4.2 Bland-Altman analysis of clinical grading (C) and automated grading (G_{pred}), average grading against grading difference for all images ($n = 1-70$).

Experimental studies are conducted on a clinical data set of fluorescein-stained eye images labeled based on clinical OGS from 0 to 5, and when automated score and clinical score are compared it can be indicated that Pearson’s correlation between them is 0.981; Lin’s CCC is 0.980, 95% confidence interval (0.963–0.989) (Table 4.1). By analyzing these results, it is clearly seen that successful automatic DES diagnostic kits can be developed by working on the fluorescein-stained cornea images and implementing computational methods to assist investigators for a more objective and faster DES diagnosis in real life.

Table 4.1. Lin’s concordance results

Concordance Results	Value
Sample concordance correlation coefficient (ρ_c)	0.9803
Lower one-sided 95% CL for ρ_c	0.9668
Lower two-sided 95% CL for ρ_c	0.9633
Upper one-sided 95% CL for ρ_c	0.9884
Upper two-sided 95% CL for ρ_c	0.9895

CHAPTER 5

FUTURE WORK AND CONCLUSION

With this study, an automated grading and diagnosis system for evaluation of DES was implemented to use efficiently in real life. The implemented study also avoids the errors that might be caused by ophthalmologists' heavy workload. Also it helps the ophthalmologists in evaluations that require attention taking into account that grading of DES severity exactly is a really difficult task for visual assessment. In this study, dry eye conditions of segmented corneal regions were evaluated automatically; it became possible to predict the severity of the corneal surface damage before an operation. Thus, the ophthalmologist can decide if the operation is convenient or not for the related patient before the operation.

As conclusion, obtained results of the implemented study were evaluated by eye specialists as successful explicitly. It is shown that this computer aided diagnosis system can speed up clinical evaluation and treatment processes with a high accuracy. According to results of this study, computer-assisted evaluation of corneal staining based on computational techniques can provide more objectivity and reduce grading variability.

The data set used in this experimental study continues to grow for future studies. Experiments still continue and are improved as new data are obtained. In future study, this experimental study can be improved with more data and different computational techniques, also.

CHAPTER 6

DISCUSSION

The use of imaging techniques and computational methods to estimate clinical score in automatically way has been already needed in medical diagnosis problems, such as some corneal disorders. These computational methods can be used for biomedical data analysis in clinics, as well as the providing of standardization of grading across multicenter traditional tests. In this way, greater precision in evaluation of treatment after-before results is provided, also a more statistically powerful dataset is obtained. Moreover, imaging these clinical data provides a detailed analysis of the treatment progress rather than traditional clinical analysis applied in ophthalmology. Analysis of past conditions can also be made in this case by creating a permanent database gradually.

In clinical trials of DES, the data acquisition of stained corneal image is relatively less common. There are some applications investigated usage of imaging data of the conjunctiva to evaluate contact lens wear in ophthalmology [71-73].

In [74] the practicability of automated grading of conjunctival disease over images was investigated to understand relation with DES. Automated analysis study of sodium fluorescein-stained digital corneal images worked on the same conjunctival disease [75].

Some assessments like automated analysis of conjunctival diseases have been observed to be especially more complex for a human investigator rather than corneal staining. Because, this complex evaluation process is based on different types of parameters such as redness intensity and vessel morphology/geometry to obtain score [76,77]. In particular, grading of dry eye disease depends on assessing number of punctate dots occurred on corneal surface after staining. Although this one-parameter approach can help grading in clinical practices, it is not exactly possible to detect the “accurate” total count of dry regions for a human investigator. The implemented study can automatically detect certain number of dry cells in both an accurate and

fast way as well as measure total staining area differing from the past studies. In case of occurrence of confluent regions, evaluation of punctate dots with manual grading based on number of punctate dots is a challenge for practical trials in clinics, and the specialist selects to rely on experience and ability to diagnose and measure the severity of DES accordingly. Automated DES analysis method can provide the grade of DES based on the OGS.

On the other hand, development of a automated diagnosis tool seems to be really useful in terms of the repeatability for the use of clinics. To be able to precisely compare clinical and automated grading performance, it must be primarily investigated whether quality of images should be kept highly by using good photography devices. Possible variations are going to be examined by working on a larger data set in future studies.

The pearson correlation coefficient between predicted score and ophthalmologist score is 0.986. There is not seen a critical bias value between predicted and ophthalmologist score according to Bland - Altman analysis. Although there may be a close agreement of differences between investigators, the clinical scores will be evaluated with a mean investigator score obtained by more investigators in future studies.

According to results of this study, though remaining a work in progress, computer assisted evaluation of corneal staining by using image processing techniques can increase objectivity and decreases scoring variability. Automated image analysis and diagnosis system shows a promising way to provide the high quality of clinical staining score and improve diagnostic outcomes in clinical trials of DES.

REFERENCES

- [1] Garcia, L.R., “*Advancing the diagnosis of Dry Eye Syndrome: development of dynamic, automated tear film Break-Up assessment*”, Thesis (PhD), Universidade Da Coruna, Faculdade de Informatica, Departamento de Computacion, 2014.
- [2] Hughes, M. S., “*Dictionary of eye terminology*”, Archives of Ophthalmology, 109(9), 1207-8, 1991.
- [3] Sullivan, D.A., & Stern, M.E., & Tsubota, K., & Dartt, D.A., & Sullivan, R.M., & Bromberg, B.B, “*Lacrimal Gland Tear Film, and Dry Eye Syndromes 3*”. (1st ed.), Springer, (Part B), US, 2002.
- [4] Lemp, M.A., “*Basic principles and classifications of dry eye disorders, in: The Dry Eye: A comprehensive Guide*”, Springer-Verlag, Berlin, 1992.
- [5] Acharya, U.R., & Ng, E.Y.K., & Suri, J. S., & Campilho, A, (Eds.), “*Image Analysis and Modeling in Ophthalmology*”, (1st ed.), CRC Press, 294-9, 2014.
- [6] Lin, H., & Yiu, S. C., “*Dry eye disease: A review of diagnostic approaches and treatments*”, Saudi Journal of Ophthalmology, 28(3), 173–181, 2014.
- [7] Foulks, G. H., & Lemp, M. A., & Vester, J. V., & Sutphin, J., & Murube, J., & Novack, G. D., “*The definition and classification of dry eye disease: Report of the Definition and Classification Subcommittee of the International Dry Eye Workshop*”, The Ocular Surface, 5,75–92, 2007.
- [8] Begley, C. G., & Chalmers, R. L., & Abetz, L., & Venkataraman, K., & Mertzanis, P., & Caffery, B.A., & Snyder, C., & Edrington, T., & Nelson, D., & Simpson, T., “*The relationship between habitual patient-reported symptoms and clinical signs among patients with dry eye of varying severity*”, Investigative Ophthalmology & Visual Science, 44, 4753-61, 2003.
- [9] Adatia, F.A., & Michaeli-Cohen, A., & Naor, J., & Caffery, B., & Slomovic, A., “*Correlation between corneal sensitivity, subjective dry eye symptoms and corneal staining in Sjogren’s syndrome*”, Canadian Journal of Ophthalmology, 39, 767-71, 2004.
- [10] Vitale, S., & Goodman, L. A., & Reed, G. F., & Smith, J. A., “*Comparison of the NEI-VFQ and OSDI questionnaires in patients with Sjogren’s syndrome-related dry eye*”, Health and Quality of Life Outcomes, 2(44), 2004.

- [11] Liu, Z., & Pflugfelder, S. C., “*Corneal surface irregularity and the effect of artificial tears in aqueous tear deficiency*”, *Ophthalmology*, 106(5), 939-43, 1999.
- [12] Goto, E., & Yagi, Y., & Matsumoto, Y., & Tsubota K. “*Impaired functional visual acuity of dry eye patients*”, *American Journal of Ophthalmology*, 133(2), 181-6, 2002.
- [13] Bron, A. J., “*Diagnosis of dry eye*”, *Survey of Ophthalmology*, 221-6, 2001.
- [14] Goto, T., & Zheng, X., & Klyce, S. D., & Kataoka, H., & Uno, T., & Karon, M., & Tatematsu, Y., & Bessyo, T., & Tsubota, K., & Obashi, Y., “*A new method for tear film stability using videokeratography*”, *American Journal of Ophthalmology*, 135(5), 607-12, 2003.
- [15] Gilbard, J. P., “*Human tear film electrolyte concentrations in health and dry-eye disease*”, *International Ophthalmology Clinics*, 34(1), 27-36, 1994.
- [16] Murube, J., “*Tear osmolarity*”, *The Ocular Surface*, 4(2), 62-73, 2006.
- [17] Tomlinson, A., & Khanal, S., & Ramaesh, K., & Diaper, C., & McFadyen, A., “*Tear film osmolarity: determination of a referent for dry eye diagnosis*”, *Investigative Ophthalmology & Visual Science*, 47(10), 4309-15, 2006.
- [18] Tsubota, K., & Fujihara, T., & Saito, K., & Takeuchi, T., “*Conjunctival epithelium expression of HLA-DR in dry eye patients*”, *Ophthalmologica*, 213(1), 16-9, 1999.
- [19] Fenga, C., & Aragona, P., & Cacciola, A., & Spinelà, R., & Nola, C. D., & Ferreri, F. & Rania, L., “*Melbonian gland dysfunction and ocular discomfort in video display terminal workers*”, *Eye*, 22:91–95, 2008.
- [20] Garc’ia-Res’ua, C., & Lira, M., & Yebra-Pimentel, E., “*Evaluaci’ on superficial en j’ovenes universitarios*”, *Rev. Esp. Contact*, 12:37–41, 2005.
- [21] Kaštelan, S., & Tomić, M., & Salopek-Rabatić, J., & Novak, B. “*Diagnostic Procedures and Management of Dry Eye*”, *BioMed Research International*, 2013, 1-6, 2013.
- [22] Tutt, R., & Bradley, A., & Begley, C., & Thibos, L.N., “*Optical and visual impact of tear break-up in human eyes*”, *Investigative Ophthalmology & Visual Science*, 41, 4117-23, 2000.

- [23] Stevenson, W., & Chauhan, S., & Dana, R. “*Dry eye disease: an immunemediated ocular surface disorder*”, *Archives of Ophthalmology*, 130(1), 90–100, 2012.
- [24] Asbell, P., & Lemp, M., “*Dry Eye Disease: The Clinician's Guide to Diagnosis and Treatment*”, (1st ed.). TNY, (Chapter 1), 2006.
- [25] John, J., & Cush, M.D. & Arthur, F., & Kavanaugh, M.D., Michael Stein, C., “*Rheumatology: Diagnosis and Therapeutics Second Edition*”, LWW, 98-99, 2004.
- [26] Vashisht, S., & Singh, S., “*Evaluation of Phenol Red Thread test versus Schirmer test in dry eyes: A comparative study*”, *International Journal of Applied and Basic Medical Research*, 1(1), 40–42, 2011.
- [27] [Ziyaret Tarihi : 5 May 2015], DEWS Reports, “*Methodologies to diagnose and monitor dry eye disease: report of the Diagnostic Methodology Subcommittee of the International Dry Eye WorkShop* pp. 108-52 [online]” <http://www.tearfilm.org/dewsreport/pdfs/TOS-0502-DEWS-noAds.pdf>
- [28] Bron, A.J., “*The Doyne Lecture. Reflections on the tears*”, *Eye (Lond)*, 11, 583-602, 1997.
- [29] Bron, A., & Evans, V. E., & Smith, J. A., “*Grading of corneal and conjunctival staining in the context of other dry eye tests*”, *Cornea*, 22(7), 640-50, 2003.
- [30] Rodriguez, J. D., & Lane, K. J., & Ousler, G. W., & Angjeli, E., & Smith, L. M., & Abelson, M. B., “*Automated grading system for evaluation of superficial punctate keratitis associated with dry eye*”, *Investigative Ophthalmology & Visual Science*, 56, 2340–7. 2015.
- [31] King-Smith, P. E., & Fink, B. A., & Fogt, N., “*Three interferometric methods for measuring the thickness of layers of the tear film*”, *Optometry and Vision Science*, 76(1), 19–32, 1999.
- [32] Goto, E., & Dogru, M., & Kojima, T., & Tsubota, K., “*Computer-synthesis of an interference color chart of human tear lipid layer, by a colorimetric approach*”, *Investigative Ophthalmology & Visual Science*, 44(11), 4693–7, 2003.
- [33] Remeseiro, B., & Ramos, L., & Penas, M., & Mart´inez, E., & Penedo, M., & Mosquera, A., “*Colour texture analysis for classifying the tear film lipid layer: a comparative study*” *International Conference on Digital Image Computing: Techniques and Applications (DICTA)*, 268–73, 2011.

- [34] Remeseiro, B., & Bolon-Canedo, V., & Peteiro-Barral, D., & Alonso-Betanzos, A., & Guijarro-Berdinas, B., & Mosquera, A., & Penedo, M. G., & S´anchez-Marro˜no, N., “*A Methodology for Improving Tear Film Lipid Layer Classification*”, IEEE Journal of Biomedical and Health Informatics, 18(4), 1485–93, 2014.
- [35] Remeseiro, B., & Mosquera, A., & Gonzalez Penedo, M., “*CASDES: a computer-aided system to support dry eye diagnosis based on tear film maps*”, Journal of Biomedical and Health Informatics, 1(1), 2015.
- [36] Ramos, L., & Barreira, N., & Mosquera, A., & Penedo, M. G., & Yebra-Pimentel, E., & Garc´ıa-Res´ua, C., “*Analysis of parameters for the automatic computation of the tear film Break-Up Time test based on CCLRU standards*”, Computer Methods and Programs in Biomedicine, 113(3), 715–24, 2014.
- [37] Remeseiro, B., & Bolon-Canedo, V., & Peteiro-Barral, D. A., & Alonso-Betanzos, Guijarro-Berdi˜nas, B., & Mosquera, A., & Penedo, M. G. & S´anchez-Marro˜no, N. “*A Methodology for Improving Tear Film Lipid Layer Classification*”, IEEE Journal of Biomedical and Health Informatics, 18(4), 1485-93, 2014.
- [38] Arslan, A., & Şen, B., & Delen, D., & Uysal, B. S., & Çelebi, F. V., & Çakmak, H. B. “*A Computer-Aided Grading System for Clinical Evaluation of Dry Eye Syndrome*”, Proceedings of the Global Conference on Healthcare Systems Engineering and Management 2016, Istanbul, Turkey, 2016.
- [39] Remeseiro, B., & Ramos, L., & Barreira, N., & Mosquera, A., & Yebra-Pimentel, E., “*Colour Texture Segmentation of Tear Film Lipid Layer Images*”, LNCS: Computer Aided Systems Theory, Revised Selected Papers EUROCAST 2013, 8112, 140–7, 2013.
- [40] Carpena, A., & Ramos, L., & Barreira, N., & Penedo, M. G., & Pena-Verdeal, H., & Gir´aldez, M. J., “*On the Automation of the Tear Film Non-Invasive Break-Up Test*”, 2th International Symposium on Computer-Based Medical Systems (CBMS), USA, 185–8, 2014.
- [41] Chun, Y. S., & Yoon, W. B., & Kim, K. G., & Park, I. K. “*Objective Assessment of Corneal Staining Using Digital Image Analysis*”, Investigative Ophthalmology & Visual Science, 55(12), 7896-903, 2014.

- [42] Acharya, U. R., & Tan, J. H., & Koh, J. E. W., & Tong, L., “*Automated Diagnosis of Dry eye using Infrared Thermography Images*”, *Infrared Physics & Technology*, 71, 263-271, 2015.
- [43] Remeseiro, B., & Mosquera, A., Penedo, M., & Garc’ia-Res’ua, C., “*Tear film maps based on the lipid interference patterns*”, 6th International Conference on Agents and Artificial Intelligence (ICAART), France, 732–9. 2014.
- [44] Wu, D., & Boyer, K. L., & Nichols, J. J., & King-Smith, P. E., “*Texture based pre lens tear film segmentation in interferometry images*”, *Machine Vision and Applications*, 21, 253-9, 2010.
- [45] Arslan, A., & Şen, B., & Çelebi, F.Ç., & Sertbaş, S. “*Automatic Segmentation of Region of Interest for Dry Eye Disease Diagnosis System*”, *Signal Processing and Communications Applications Conference*, SIU 2016, Zonguldak.
- [46] [Ziyaret Tarihi: 5 May 2015] Topcon Medical, “Products-DC3 [online]” <http://www.topconmedical.com/products/dc3.htm>
- [47] Devi, G. D., & Preethi, D.M.D, “*Disease Identification in Iris Using Gabor Filter*”, *International Journal Of Engineering And Computer*, 3(4), 5396-9, 2014.
- [48] Mahlouji, M., & Noruzi, A., “*Human Iris Segmentation for Iris Recognition in Unconstrained Environments*”, *IJCSI International Journal of Computer Science Issues*, 9(1), 2012.
- [49] Adegoke, B. O., & Omidiora, E. O, & Falohun, S. A. & Ojo, J.A., “*Iris Segmentation: a survey*”, *International Journal of Modern Engineering Research (IJMER)*, 3(4), 1885-9, 2013.
- [50] Masek, L., “*Recognition of Human Iris Patterns for Biometric Identification*”, *School of Computer Science and Software Engineering*, The University of Western Australia, 2003.
- [51] Radu, P., & Sirlantzis, K., & Howells, G., & Hoque, S., & Deravi, F., “*A Colour Iris Recognition System Employing Multiple Classifier Techniques*”, *Electronic Letters on Computer Vision and Image Analysis*, 12(2), 54-65; 2013.
- [52] Arvacheh, E. M. & Tizhoosh, H. R., “*IRIS Segmentation: Detecting Pupil, Limbus and Eyelids*”, 2006 International Conference on Image Processing, Atlanta, GA, 2006, 2453-6.

- [53] Yedidya, T., & Hartley, R., & Guillon, J.P., & Kanagasingam, Y., “*Automatic dry eye detection*”, Proceedings of the 10th international conference on Medical image computing and computer-assisted intervention, Ayache, N., & Ourselin, S., & Maeder, A. (Eds.), Vol. Part I. Springer-Verlag, Berlin, Heidelberg, 792-799. 2007.
- [54] Sharma, K., & Monga, H., “*Efficient Biometric Iris Recognition Using Hough Transform With Secret Key*”, International Journal of Advanced Research in Computer Science and Software Engineering, 4(7), 632-40, 2014.
- [55] Daugman, J., “*How iris recognition works*”, Proceedings of 2002 International Conference on Image Processing, 1,16-22, 2002.
- [56] Ritter, N., “*Location of the pupil-iris border in slit-lamp images of the cornea*”, Proceedings of the International Conference on Image Analysis and Processing, 1999.
- [57] Desoky, A. I., & Ali, H. A., & Abdel-Hamid, N. B. “*Enhancing iris recognition system performance using templates fusion*”, The 10th IEEE International Symposium on Signal Processing and Information Technology, Luxor, 451-456, 2010.
- [58] Wojcikiewicz, W., “*Hough Transform, Line Detection in Robot Soccer*”, Coursework for Image Processing, 2008.
- [59] Cherabit, N., & Chelali, F. Z., Djeradi, A., “*Circular Hough Transform for Iris localization*”, Science and Technology, 2(5), 114-121, 2012.
- [60] Dubey, A. B., & Madan, A., “*Iris Localization using Daugman’s Inter-Differential Operator*”, International Journal of Computer Applications, 93(3), 2014.
- [61] Kong, W., & Zhang, D. “*Accurate iris segmentation based on novel reflection and eyelash detection model*”, Intelligent Multimedia, Video and Speech Processing, 2004. Proceedings of 2004 International Symposium on, 2001.
- [62] Tisse, C., & Martin, L., & Torres, L. & Robert, M., “*Person identification technique using human iris recognition*”, International Conference on Machine Vision and Human-Machine Interface, 2002.
- [63] Ma, L., & Wang, Y., & Tan, T., “*Iris recognition using circular symmetric filters*”, National Laboratory of Pattern Recognition, Institute of Automation, Chinese Academy of Sciences, 2002.

- [64] Singh, S., & Datar, A., “*EDGE Detection Techniques Using Hough Transform*”, International Journal of Emerging Technology and Advanced Engineering, 3(6),2013.
- [65] Wildes, R., & Asmuth, J., & Green, G., & Hsu, S., & Kolczynski, R., & Matey, J., & McBride, S., “*A system for automated iris recognition*”, Proceedings IEEE Workshop on Applications of Computer Vision, Sarasota, FL, 121-8, 1994.
- [66] Mohamed, M. A., Abou-El-Soud, M. A., & Eid, M. M., “*Iris Detection and Normalization in Image Domain Based on Morphological Features*, IJCSI International Journal of Computer Science Issues, 11(1), 51-59, 2014.
- [67] Labati, R.D., & Scotti, F., “*Noisy iris segmentation with boundary regularization and reflections removal*”, Image and Vision Computing 28, 270-7, 2010.
- [68] Gonzales, R. C., & Woods, R. E., & Eddins, S. L., “*Digital Image Processing Using Matlab*”, (2n ed.). Gatesmark, (Chapter 9), 2009.
- [69] Iverson, J., & Kamath, C., & Karypis, G. “*Evaluation of connected component labeling algorithms for distributed-memory systems*”, Parallel Computing, 44, 53-68. 2015.
- [70] Lin L., “*A concordance correlation coefficient to evaluate Reproducibility*”, Biometrics,45, 225–68,1989.
- [71] Altman, D.G., Bland, J.M., “*Measurement in medicine: the analysis of method comparison studies*”, Statistician, 32, 307–17, 1983.
- [72] Efron, N., Morgan, P.B., Katsara, S.S., “*Validation of grading scales for contact lens complications*”, Ophthalmic and Physiological Optics, 21,17–29,2001.
- [73] Efron N., “*Grading scales for contact lens complications*”, Ophthalmic and Physiological Optics,18, 182–6,1998.
- [74] Rodriguez, J.D., & Johnston, P.R., & Ousler G.W., & Smith, L.M., & Abelson, M.B., “*Automated grading system for evaluation of ocular redness associated with dry eye*”, Journal of Clinical Ophthalmology,7,1–8, 2013.
- [75] Yoneda, T., & Sumi, T., & Takahashi, A. “*Automated hyperemia software analysis: reliability and reproducibility in healthy subjects*”. Japanese Journal of Ophthalmology, 56, 1–7, 2012.

[76] Fieguth, P., & Simpson, T., “*Automated measurement of bulbar Redness*”, Investigative Ophthalmology & Visual Science, 43, 340–7, 2002.

[77] Papas, E.B., “*Key factors in the subjective and objective assessment of conjunctival erythema*”, Investigative Ophthalmology & Visual Science, 41, 687–91, 2000.



APPENDICES

Appendix A Grading Example 1

Appendix B Grading Example 2



APPENDIX A Grading Example 1

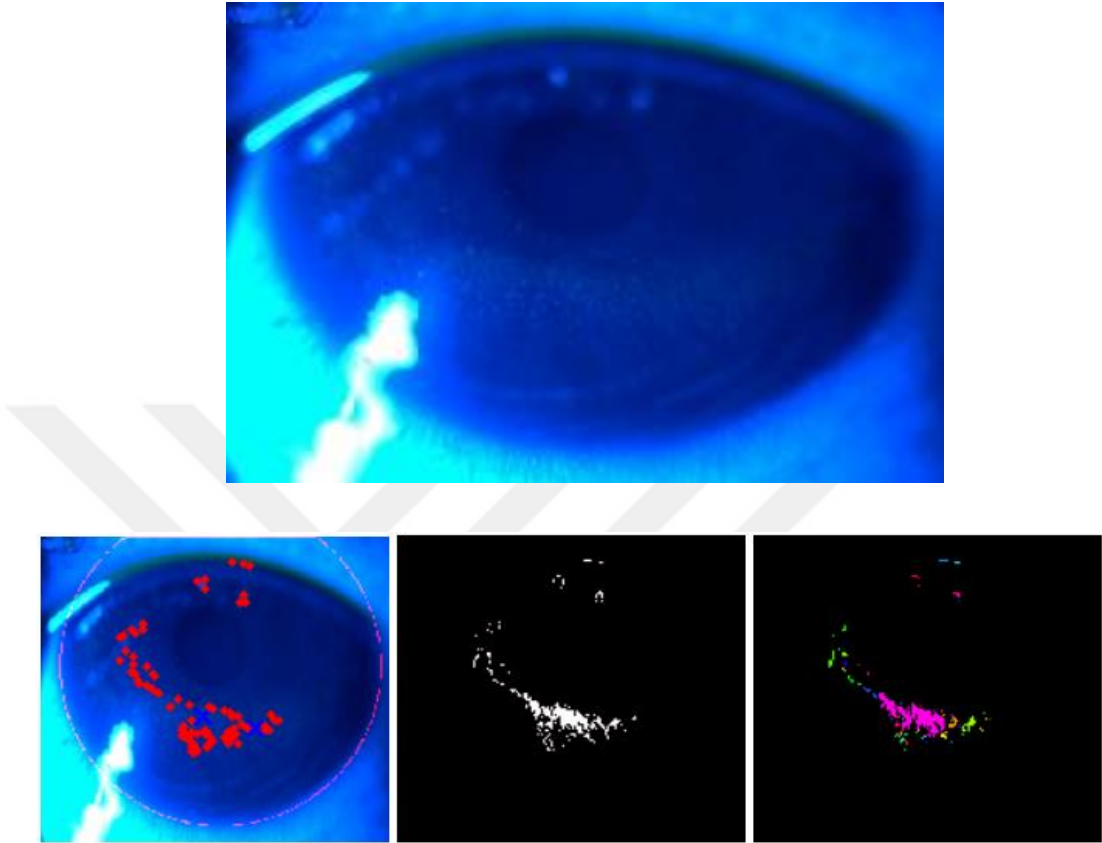


Figure A.1 Grading a sample in grade 3 based on counted dot number and area

Table A.1. Quantative analysis results of each dry blob reported at the end of computational methods in Figure A.1 and grading as grade 3

Blob Number	Mean Intensity	Area	Perimeter	Centroid		Diameter
1	26.6	36.0	38.7	73.2	114.1	6.8
2	26.0	2.0	2.0	74.5	92.0	1.6
3	26.0	1.0	0.0	78.0	90.0	1.1
4	26.0	2.0	2.0	79.5	105.0	1.6
5	26.1	15.0	12.5	85.3	109.5	4.4
6	26.4	11.0	15.1	85.1	85.4	3.7
7	26.1	13.0	13.1	85.5	116.9	4.1
8	26.0	5.0	9.7	84.6	123.6	2.5
9	26.0	1.0	0.0	88.0	89.0	1.1
10	26.3	4.0	6.0	88.0	125.5	2.3
11	26.0	3.0	4.0	89.0	130.0	2.0
12	26.0	6.0	9.7	92.0	133.7	2.8
13	26	2	2	95	80.5	1.6
14	26.5	2	2	95	84.5	1.6
15	26	2	2	97.5	119	1.6
16	26	5	7.7	98.4	136	2.5
17	26	1	0	103	140	1.1
18	26	1	0	104	126	1.1
19	27.4	24	33.6	109.5	143.8	5.5
20	26	2	2	106	126.5	1.6
21	25.5	707	410.6	148.4	164.9	30.0
22	29.2	5	6.8	119.4	155.4	2.5
23	26	1	0	127	149	1.1
24	26.9	17	20.5	132.4	172.6	4.7
25	26	1	0	130	176	1.1
26	26	3	4.8	130.3	182	2.0
27	27	2	2	132	178.5	1.6
28	26	4	6.2	133.5	183.3	2.3
29	26.3	21	34.1	137.4	185.8	5.2
30	26	1	0	136	154	1.2
31	26	3	4	136	181	2.0
32	26	3	4	138	178	2.0
33	26	1	0	138	168	1.1
34	26	1	0	139	191	1.1
35	26	4	5.4	139.2	195.3	2.3
36	26.3	9	10.8	141	188.3	3.4
37	26	1	0	141	198	1.3
38	26	1	0	142	192	1.3
39	26	1	0	143	179	1.3
40	26.6	3	4.8	144.3	42	2.0
41	26	2	2	144	195.5	1.6
42	27.2	12	25.3	150.6	40.4	4.0
43	26	1	0	149	178	1.1
44	26	1	0	150	176	1.1
45	26	1	0	150	180	1.1

46	27.8	4	4.8	151.5	48	2.3
47	26	2	2	152	178.5	1.6
48	26	2	2.8	153.5	155.5	1.6
49	26	1	0	153	192	1.1
50	26	1	0	154	188	1.1
51	26	4	6.2	156	183.8	2.3
52	26	2	2	158	156.5	1.6
53	26	4	6.8	158.5	187.5	2.3
54	26	1	0	168	184	1.1
55	26	1	0	169	159	1.1
56	26	1	0	170	184	1.1
57	26.9	8	14	174.5	24	3.2
58	26	2	2.8	172.5	178.5	1.6
59	26,56	25	35.2	175.5	183.2	5.6
60	26	1	0	172	188	1.1
61	26	1	0	173	161	1.1
62	26.3	3	4.8	175	163.7	2.0
63	26	1	0	177	175	1.1
64	26	3	4.8	178.3	180	2.0
65	26.6	48	54.5	183.3	170.5	7.9
66	26	3	4.8	181.3	164	2.0
67	26	1	0	181	189	1.1
68	27	7	12.8	185	25.6	3.0
69	26.9	18	22.7	185.7	54.6	4.8
70	26.7	3	4.8	182.3	61	2.0
71	26	2	2.8	187.5	61.5	1.6
72	26	5	7.7	188.6	174.6	2.5
73	26	2	2	191.5	27	1.6
74	26.4	80	78.8	196.7	174	10.1
75	26	2	2.8	204.5	174	1.6
76	26	1	0	205	177	1.1
77	26.3	3	4.8	208.7	177	2.0
78	26	1	0	211	162	1.1
79	26	1	0	213	168	1.1
80	26	5	5.4	216.6	167.2	2.5

APPENDIX B Grading Example 2

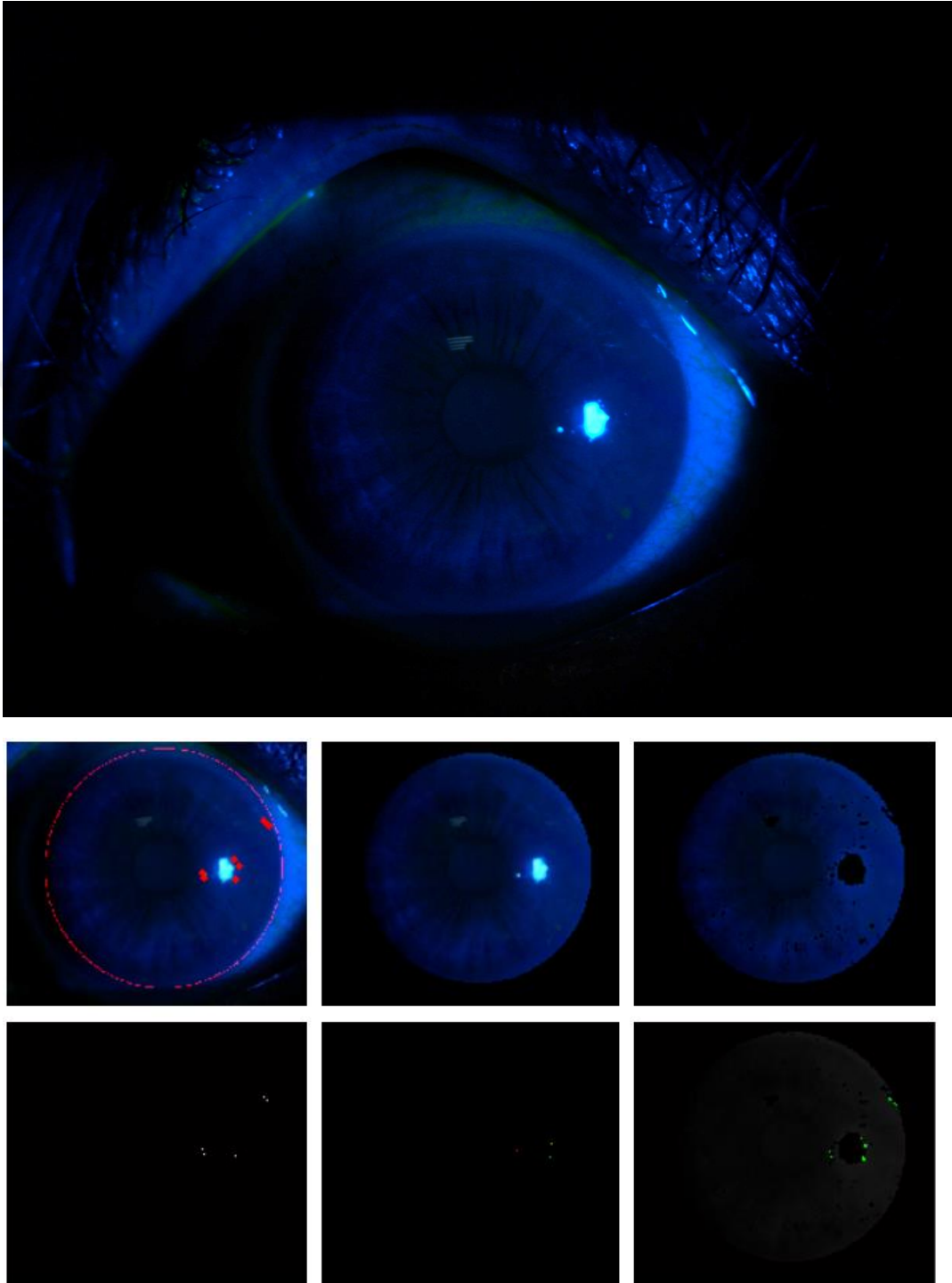


Figure B.1 Grading a sample in grade 1 based on counted dot number and area

Table B.1 Quantative analysis results of each dry blob reported at the end of computational methods in Figure A.2 and grading as grade 1

Blob Number	Mean Intensity	Area	Perimeter	Centroid	Diameter	Blob Number
1	27	1	0	209	138	1.1
2	28	1	0	210	143	1.1
3	26	1	0	242	123	1.1
4	26.2	5	6.8	244	145	2.5
5	26	2	2.8	246.5	131.5	1.6
6	26	2	2.8	272.5	83.5	1.6
7	26	1	0	277	87	1.1
8	27	1	0	279	88	1.1



RESUME

Research Assistant Ayşe ARSLAN

Faculty of Engineering and Natural Sciences
Yildirim Beyazıt University, Ankara, Turkey
E-mail: aarslan@ybu.edu.tr
Web: <http://ybu.edu.tr/aarslan/>

EDUCATION

MS, 2015, Department of Computer Engineering, Yildirim Beyazıt University, Ankara, Turkey
GPA:4.00/4.00

Thesis: Automated Grading and Diagnosis System for Evaluation of Dry Eye Disease

BS, 2013, Department of Computer Engineering, Gazi University, Ankara, Turkey
GPA:3.16/4.00

Thesis: Cardiac Arrhythmia Analysis Using Hidden Markov Model and Murmur Diagnosis

WORK EXPERIENCE

Yildirim Beyazıt University - Research Assistant (2014-)
Department of Computer Engineering

Siemens Enterprise Communications - Software Engineer (2013-2014)
Project: Software Development and Maintenance of Siemens Openstage Phone Firmwares

Tek-sis Advanced Technologies - .NET Programmer (2013)
Project: Software Development for Renewable Energy Test Control Devices of Fuel Cell Production

RESEARCH INTEREST

Machine Learning, Data Mining, Decision Support Systems, Biomedical Data Analysis, Signal and Image Processing, Parallel Programming with CUDA.

PUBLICATIONS

1) Arslan, A.; Yıldız, O., "*Cardiac Arrhythmia Analysis Using Hidden Markov Model and Murmur Diagnosis*", Signal Processing and Communications Applications Conference, SIU 2014, Trabzon.

- 2) Arslan, A.; Şen, B., “**Detection of Non-Coding RNA’s with Optimized Support Vector Machines**”, Signal Processing and Communications Applications Conference, SIU 2015, Malatya.
- 3) Arslan, A.; Şen, B.; Çelebi, F. V.; Peker, M.; But, A.; “**A Comparison of Different Classification Algorithms For Determining The Depth of Anesthesia Level on A New Set of Attributes**”, 2015 International Symposium on INnovations in Intelligent SysTems and Applications, Madrid, Spain.
- 4) Peker, M.; Arslan, A.; Şen, B.; Çelebi, F. V.; But, A.; “**A Novel Hybrid Method for Determining the Depth of Anesthesia Level: Combining ReliefF Feature Selection and Random Forest Algorithm (ReliefF+RF)**”, 2015 International Symposium on INnovations in Intelligent SysTems and Applications, Madrid, Spain.
- 5) Arslan, A.; Şen, B.; Çelebi, F. V.; Sertbaş, S.; “**Automatic Segmentation of Region of Interest for Dry Eye Disease Diagnosis System**”, Signal Processing and Communications Applications Conference, SIU 2016, Zonguldak.
- 6) Arslan, A.; Şen, B.; Delen, D.; Uysal, B. S.; Çelebi, F. V.; Çakmak, H. B.; “**A Computer-Aided Grading System for Clinical Evaluation of Dry Eye Syndrome**”, Proceedings of the Global Conference on Healthcare Systems Engineering and Management 2016, Istanbul, 2016.
- 7) Arslan, A.; Şen, B.; Delen, D.; Çelebi, F. V.; “**Implementation of Computer Assisted Voice Search Engine for Medical Transcription**”, Proceedings of the Global Conference on Healthcare Systems Engineering and Management 2016, Istanbul, 2016.